Chemical Geology 389 (2014) 137–152

Contents lists available at ScienceDirect

Chemical Geology

journal homepage: www.elsevier.com/locate/chemgeo

Fingerprints of metamorphism in chromite: New insights from minor and trace elements

Vanessa Colás [a,b,*], José M. González-Jiménez [b,c], William L. Griffin [b], Isabel Fanlo [a], Fernando Gervilla [d], Suzanne Y. O'Reilly [b], Norman J. Pearson [b], Thomas Kerestedjian [e], Joaquín A. Proenza [f]

[a] Universidad de Zaragoza, Departamento de Ciencias de la Tierra, Pedro Cerbuna 12, 50009 Zaragoza, Spain
[b] Australian Research Council Centre of Excellence for Core to Crust Fluid Systems/GEMOC, Department of Earth and Planetary Sciences, Macquarie University, Sydney, NSW 2109, Australia
[c] Departamento de Geología, Andean Geothermal Center of Excellence (CEGA), Universidad de Chile, Santiago, Chile
[d] Departamento de Mineralogía y Petrología and Instituto Andaluz de Ciencias de la Tierra (Universidad de Granada-CSIC), Facultad de Ciencias, Avda. Fuentenueva, s/n, 18002 Granada, Spain
[e] Geological Institute, Bulgarian Academy of Sciences, 24 Georgi Bonchev Str., 1113 Sofia, Bulgaria
[f] Departament de Cristal lografia, Mineralogia i Dipòsits Minerals, Facultat de Geologia, Universitat de Barcelona, Martí i Franquès, s/n, 08028 Barcelona, Spain

ARTICLE INFO

Article history:
Received 8 April 2014
Received in revised form 1 October 2014
Accepted 2 October 2014
Available online 13 October 2014

Editor: L. Reisberg

Keywords:
Chromite
Metamorphism
Laser-ablation ICP-MS
Mobility of minor and trace element
Rhodope metamorphic complex

ABSTRACT

A suite of minor and trace elements (Ga, Ti, Ni, Zn, Co, Mn, V, Sc) in chromite grains from ophiolitic chromitites subjected to high-pressure metamorphism defines a metamorphic signature. A two-stage process associated with the infiltration of fluids during retrograde metamorphism from eclogite- to amphibolite-facies has produced four types of chromites: (1) *porous chromite* strongly enriched in Cr and Fe^{2+} but depleted in Al and Mg, with abundant chlorite filling the pores; (2) *non-porous chromite* strongly enriched in Fe^{3+} (i.e., ferrian chromite); (3) *partly altered chromite* with primary cores surrounded by chlorite-bearing porous chromite; and (4) *zoned chromite* made up of primary cores surrounded by non-porous rims of ferrian chromite.

Compared to spinels from unmetamorphosed chromitites the cores of partly altered chromites after primary high-Cr chromite are enriched in Zn, Co and Mn but strongly depleted in Ga, Ni and Sc. This distribution of minor- and trace-elements is related to a decrease in Mg# [Mg/(Mg + Fe^{2+})] and Al, produced by the crystallization of chlorite in the pores of porous chromite. Non-porous chromite is enriched in Ti, Ni, Zn, Co, Mn and Sc but depleted in Ga, suggesting that fluid-assisted processes have obliterated the primary magmatic signature. Zoned chromites have cores depleted in Ga, Ni and Sc but are progressively enriched in Zn, Co and Mn as Mg# and Al decrease toward the rims; they have overall lower concentrations in Ga, Ni and Sc and higher Zn and Co than the non-porous rims of ferrian chromite. The complex variation of the minor- and trace-elements vs $Fe^{3+}/(Fe^{3+} + Fe^{2+})$ in the different types of chromite suggests a complex interplay of substitutions, linked with the ability of fluids to infiltrate the chromite and the extent of the re-equilibration between pre-existing cores and newly-formed rims.

The results demonstrate that metamorphism can seriously disturb the original magmatic distribution of minor and trace elements in chromite. The abundances of these elements, and by inference the major elements, can be strongly modified even in the cores of grains that appear "unaltered" in terms of major elements. The use of the major elements as indicators of magmatic processes therefore must be linked to careful evaluation of metamorphic effects, using LA-ICP-MS analysis of minor and trace elements.

1. Introduction

Chromite is an oxide with a spinel-type structure that might be expressed using the general formula AB_2O_4. The A site is occupied by Mg and Fe^{2+} in tetrahedral coordination and the B site is usually occupied by Cr and Al in octahedral coordination; Cr and Al may be substituted by Fe^{3+} giving rise to *ferrian chromite*. Elements like Zn^{2+}, Co^{2+}, Mn^{2+} and Ni^{2+} can substitute Mg and Fe^{2+} in A and V^{3+}, Sc^{3+}, Ga^{3+} and Ti^{4+} can substitute Al and Cr in B (Table 1). These variations in the composition of chromite are commonly used to interpret the petrogenesis and the geodynamic setting of the host ultramafic rocks (Irvine, 1967; Dick and Bullen, 1984; Arai, 1992; Stowe, 1994; Zhou and Robinson, 1994; Barnes and Roeder, 2001; Kamenetsky et al., 2001; Ahmed et al., 2005; Rollinson, 2008; Pagé and Barnes, 2009). The high resistance of chromite to alteration (compared to the primary silicates) has made this oxide particularly useful as a petrogenetic indicator in ultramafic rocks in which metamorphic alteration has

* Corresponding author at: Universidad de Zaragoza, Departamento de Ciencias de la Tierra, Pedro Cerbuna 12, 50009 Zaragoza, Spain. Tel.: +34 976 84 10 98.
E-mail addresses: vcolas@unizar.es (V. Colás), jose.gonzalez@mq.edu.au, jmgonzj@ing.uchile.cl (J.M. González-Jiménez), bill.griffin@mq.edu.au (W.L. Griffin), fanlo@unizar.es (I. Fanlo), gervilla@ugr.es (F. Gervilla), sue.oreilly@mq.edu.au (S.Y. O'Reilly), norman.pearson@mq.edu.au (N.J. Pearson), thomas@geology.bas.bg (T. Kerestedjian), japroenza@ub.edu (J.A. Proenza).

http://dx.doi.org/10.1016/j.chemgeo.2014.10.001
0009-2541/

Table 1
Major-, minor- and trace element distribution in the different mineral structures.

	Chromite		Olivine	Chlorite	
Formula	AB_2O_4		A_2SiO_4	$(A_5Al)(Si_3Al)O_{10}(OH)_8$	
Position	$A^{(IV)}$	$B^{(VI)}$	$A^{(VI)}$	$A^{(VI)}$	$Al^{(VI)}$
Major elements	Mg^{2+}, Fe^{2+}	Cr^{3+}, Al^{3+}, Fe^{3+}	Mg^{2+}, Fe^{2+}	Mg^{2+}, Fe^{2+}	Cr^{3+}
Minor- and trace elements	Zn^{2+}, Co^{2+}, Mn^{2+}, Ni^{2+}	V^{3+}, Sc^{3+}, Ga^{3+}, Ti^{4+}	Zn^{2+}, Co^{2+}, Mn^{2+}, Ni^{2+}	Ni^{2+}	Ga^{3+}

obliterated other primary fingerprints (e.g. Proenza et al., 2004; Ahmed et al., 2005; González Jiménez et al., 2009). However, a growing body of work, based on the study of chromite-rich rocks from ophiolites, layered complexes and komatiites, has shown that the chemistry and structure of chromite can be also significantly modified during both prograde (Bliss and MacLean, 1975; Evans and Frost, 1975; Wylie et al., 1987; Frost, 1991; Burkhard, 1993; Abzalov, 1998; Barnes, 2000; González Jiménez et al., 2009; Merlini et al., 2009; Olobaniyi and Mücke, 2011) and retrograde metamorphism (Loferski, 1986; Proenza et al., 2004, 2008; Mellini et al., 2005; Mukherjee et al., 2010; Gervilla et al., 2012; Grieco and Merlini, 2012).

Metamorphism typically imposes an optical and chemical zoning on the primary chromite. In general, a zone enriched in FeO and Cr_2O_3 and depleted in MgO and Al_2O_3 surrounds the apparently pristine (or primary) core, which grades outwards to chromite strongly enriched in Fe^{3+} (ferrian chromite) (Bliss and MacLean, 1975; Evans and Frost, 1975; Wylie et al., 1987; Kimball, 1990; Barnes, 2000; Mellini et al., 2005; González Jiménez et al., 2009; Merlini et al., 2009; Mukherjee et al., 2010; Gervilla et al., 2012; Grieco and Merlini, 2012). Occasionally magnetite rims surround the cores and/or the ferrian chromite rims.

Evans and Frost (1975), Bliss and MacLean (1975) and Barnes (2000) have suggested that the ferrian chromite is produced by the reaction of pristine cores with magnetite rims during prograde metamorphism of serpentinised ultramafic rocks. In contrast, Gervilla et al. (2012) proposed that the formation of ferrian chromite is a two-stage process occurring during the retrograde evolution of chromitites from eclogite-facies conditions. During the first stage, magmatic chromite reacts with olivine in the presence of reducing fluids to produce a porous chromite enriched in FeO and Cr_2O_3 (hereafter *Fe^{2+}-rich chromite*), which is in equilibrium with chlorite. In the second stage, oxidizing solutions circulate through the network of pores in the porous chromite, dissolving chlorite and adding Fe^{3+}, which diffuses into the chromite lattice and converts it to ferrian chromite (i.e., *Fe^{3+}-rich chromite*).

Both models implicitly assume that the cores of chromite grains represent relict primary chromite that remained unaffected by the alteration. However, the selective enrichment of a suite of minor elements including Mn, Ni, Co, Zn and Ti in such "pristine cores", in metamorphosed chromites from the Tidding Suture Zone in the eastern Himalaya (Singh and Singh, 2013) and the Nuggihalli schist belt in India (Mukherjee et al., 2010) led us to investigate whether their compositions are perturbed and do not represent original pristine compositions. If so, important information about the metamorphic evolution of chromite might be lost by analyzing only microstructures and the abundances of major elements, and deductions about the original magmatic–tectonic situation of the chromitites and their host peridotites might be incorrect.

The technique of laser-ablation inductively-coupled plasma-mass spectrometry (LA-ICP-MS) has lower limits of detection than the electron microprobe and thus can analyze a more comprehensive suite of elements present in a chromite (Ga, Ti, Ni, Zn, Co, Mn, V and Sc), providing useful information about its petrogenesis (Dare et al., 2009; Pagé and Barnes, 2009; González-Jiménez et al., 2011, 2013, 2014; Aldanmaz, 2012). In this work LA-ICP-MS was used to measure the minor- and trace elements in highly metamorphosed chromites, in order to define the fingerprints of metamorphism that are not revealed by conventional approaches based on electron microprobe data. We have studied chromite from metamorphosed chromitites because they preserve zoning patterns better than accessory chromites in peridotite at a given degree of alteration (e.g. Proenza et al., 2004). The chromitites are enclosed in four ultramafic massifs (Golyamo Kamenyane, Chernichevo, Yakovitsa and Avren) representing portions of the dismembered ophiolites of the Rhodope Metamorphic Core Complex in southern Bulgaria. The chromitites and their host ultramafic rocks underwent metamorphism in eclogite facies with a later amphibolite-facies overprint (Mposkos and Krohe, 2000, 2006; Mposkos, 2002; Mposkos et al., 2012). In order to test the validity of our approach we have additionally compared our chromites with those from unaltered chromitites in unmetamorphosed ophiolites (Eastern Cuba and New Caledonia) with well-documented post-magmatic histories.

2. Sample background

The samples selected for this study are from Type I ophiolitic chromitites (i.e., enriched in IPGE relative to PPGE; González-Jiménez et al., 2014) in the metamorphosed ultramafic massifs of Golyamo Kamenyane, Chernichevo, Yakovitsa and Avren in the eastern part of the Rhodope Metamorphic Core Complex, of southern Bulgaria and northern Greece (Table 2 and Fig. 1).

The Rhodope Metamorphic Core Complex is a large domal structure formed mainly during the Alpine orogeny; it lies between the Balkan belt to the north and the Dinarides–Hellenides to the south-southwest (Fig. 1). The complex consists of (1) a lower unit corresponding to the *autochthonous core* and known as the Gneiss–Migmatite Complex (Kozhoukharov et al., 1988; Haydoutov et al., 2001), the lower High-Grade Unit (Bonev, 2006) or the Lower Allochthon (Janák et al., 2011), and (2) an upper unit with meta-ophiolites (Kolcheva and Eskenazy, 1988; Bazylev et al, 1999; Kolcheva et al., 2000; Haydoutov et al., 2001, 2004; Bonev et al., 2006; Daieva et al, 2007) which represents the *allochthonous rim* and is known as the Variegated Complex (Kozhoukharov et al., 1988; Haydoutov et al., 2001), the upper High-Grade Unit (Bonev, 2006) or the Upper Allochthon (Janák et al., 2011). In the eastern part of the Rhodope Metamorphic Core Complex, both the autochthonous core and the allochthonous rim crop out in two large-scale domal structures: the Kesebir–Kardamos Dome to the west and the Byala Reka–Kechros Dome to the east (Fig. 1; Georgiev, 2006).

The ultramafic massifs of Golyamo Kamenyane, Avren, and Chernichevo crop out in the western limb of the Byala Reka–Kechros Dome along the Avren synform (Fig. 1). The ultramafic massif of Yakovitsa crops out in the western limb of the Kesebir–Kardamos Dome (Fig. 1). These ultramafic massifs consist of partly serpentinised harzburgite and dunite, which are overlain by layers of amphibolites (i.e. formerly layered gabbros; Bazylev et al, 1999; Kolcheva et al., 2000; Haydoutov et al., 2004; Gervilla et al, 2012) in the massifs of Golyamo Kamenyane and Chernichevo. These lithologies, including chromitites, are cut by sub-vertical veins of asbestos, mainly anthophyllite and chrysotile, and talc in the massifs of Golyamo Kamenyane (Gervilla et al, 2012) and Avren (Kolkovski et al., 2003).

Mposkos and Krohe (2000, 2006) and Mposkos (2002) investigated spinel-garnet metaperidotites and garnet pyroxenites of the Kimi Complex (the Greek equivalent of the Avren synform in Bulgaria) and concluded that the mantle rocks of the allochthonous rim of the

Table 2
Characterization of the chromitite samples investigated in this study.

Locality	Sample	Size of the body (wide)	Location in the chromitite body	Texture	Chromite microstructure	Chromite grain zone	Chemical Variations		
							Cr#	Mg#	$Fe^{3+}/(Fe^{3+} + Fe^{2+})$
High-Al Chromitites									
Golyamo Kamenyane	GK1A-5	>10 m	Core	Semi-massive	Partly altered chromite	Core	0.52–0.60	0.59–0.71	<0.30
	GK1A-6								
	GK1A-7								
	GK3C-1					Porous rim	0.57–0.91	0.44–0.68	<0.28
	GK3-100								
	GK3-101								
	GK4-100								
	GK1A-4	>10 m	Core	Semi-massive	Porous chromite	Core to rim profile	0.91–0.96	0.35–0.48	0.21–0.53
	GK3A-1								
	GK1C-3	>10 m	Shear zone	Massive	Zoned chromite	Core	0.62–0.69	0.49–0.57	0.10–0.34
						Non-porous rim	0.83–0.99	0.20–0.36	0.49–0.63
	GK1C-1	>10 m	Shear zone	Massive	Non-porous chromite	Core to rim profile	0.96–0.99	0.16–0.32	0.55–0.66
	GK1C-2								
Chernichevo	CH1-4	>1 m	Core	Semi-massive	Partly altered chromite	Core	0.55	0.59	0.31
						Porous rim	0.58–0.65	0.51–0.57	0.27–0.32
High-Cr Chromitites									
Yakovitsa	J1-H1	30–40 cm	Core	Massive	Partly altered chromite	Core	0.71–0.78	0.59–0.69	0.07–0.26
	J1-E2								
	J1-B7		Core			Porous rim	0.78–0.97	0.45–0.66	0.18–0.43
	J1-B6		Rim	Semi-massive					
	J1-B2								
	J1-D1	20–30 cm	Core	Disseminated	Partly altered chromite	Core	0.60–0.83	0.40–0.65	0.05–0.29
	J1-F1					Porous rim	0.78–0.98	0.29–0.46	0.31–0.50
	J1-G2								
	J1-A3	<20 cm	Core	Disseminated	Zoned chromite	Core	0.68–0.73	0.38–0.42	0.08–0.17
						Non-porous rim	0.91–0.98	0.16–0.27	0.43–0.61
Avren	AV3-117	1–2 m	Core	Massive	Zoned chromite	Core	0.84–0.93	0.35–0.46	0.19–0.31
	AV3-110		Core to rim	Semi-massive					
	AV3					Non-porous rim	0.93–0.98	0.08–0.35	0.50–0.67
	AV3-121		Rim	Disseminated					

Complex have undergone ultra-high pressure (UHP)/high temperature (HT) metamorphism (>25 kbar and >1,200 °C), and a later overprinting in eclogite- or granulite-facies (13.5–16 kbar and 750–775 °C). An amphibolite-facies (~10 kbar and 600–650 °C) overprint is also recorded in metasediments spatially associated with the mantle rocks (Mposkos and Krohe, 2000, 2006; Mposkos, 2002). Mposkos et al. (2012) have estimated a somewhat similar retrograde metamorphic pathway in the rocks of the Gneiss–Migmatite Complex: from ultra-high pressures (22.8–20.6 kbar) but lower temperatures (617–553 °C), to eclogite-facies (15.2–18.6 kbar and 672–566 °C), with amphibolite-facies overprint (6.6–8.8 kbar and 570–498 °C).

The investigated chromitite samples were collected from small chromitite pods and layers, with lengths of a few tens of meters and thicknesses between <0.5 m and 2 m, except in Golyamo Kamenyane where chromitite bodies are a few hundred meters long and tens of meters thick. Samples of massive, semi-massive and disseminated chromitites were collected from chromitite bodies of variable size (Table 2).

Gervilla et al. (2012) showed that in the Golyamo Kamenyane chromitites, the metamorphism has produced four microstructural types of chromites (Table 2; Fig. 2a–f): (1) *partly altered chromite* with primary cores surrounded by porous chromite rims; (2) *porous chromite* in which abundant pores are filled by chlorite; (3) *zoned chromite* in which coarse grains have primary cores, sharply separated from a non-porous chromite rim; (4) *non-porous chromite*, which hosts some inclusions of chlorite and minor antigorite, and shows a polygonal mosaic microstructure.

We re-examined the Golyamo Kamenyane chromitites and observed that the partly altered chromites dominate the central parts of the chromitite pods, whereas porous chromite is mainly found at the edges or highly fractured areas. Zoned chromite and non-porous chromite were only found along shears and fault zones cutting the chromitite bodies. Partly altered chromite is also preserved in the small chromitite bodies in the massifs of Yakovitsa and Chernichevo, whereas zoned chromite is found in sheared disseminated chromitites from Yakovitsa and Avren massifs (Table 2; Fig. 2a–f). The chromite grains are predominantly subhedral and less frequently anhedral with a characteristic rounded shape. Individual grains may have a fracture network of variable density; in the massive chromitites of Golyamo Kamenyane this network was produced by shearing along faults cutting the chromitite bodies. In the chromitite bodies of Chernichevo these fractures are often filled with magnetite.

3. Analytical techniques

Selected chromite grains preserving the metamorphic patterns described above were imaged using a scanning electron microscope (SEM) model JEOL SM 6400 SEM at University of Zaragoza, Spain.

Major (Mg, Al, Cr, Fe and Si) and minor (Ti, V, Mn, Zn and Ni) elements in chromite were analyzed using a CAMECA SX-50 electron microprobe at Serveis Científico Técnics of University of Barcelona, Spain. The analytical conditions were 20 kV accelerating voltage, 20 nA beam current, and beam diameter of 3 μm. Counting times were 20 s on TAP/PET and 30 s on LiF crystals. ZAF corrections were applied online. The following spectral lines were monitored: Mg Kα, Al Kα, Si Kα with the TAP diffracting crystal, Ti Kα and Cr Kα with the PET diffracting crystal, and V Kα, Mn Kα, Fe Kα, Ni Kα and Zn Kα with the LiF diffracting crystal. Calibration standards were natural and synthetic materials: periclase (Mg), Al_2O_3 (Al), Cr_2O_3 (Cr), Fe_2O_3 (Fe), diopside (Si), rutile (Ti), pure V, rhodonite (Mn), NiO (Ni), and sphalerite (Zn). Structural formulae of Cr-spinel were calculated assuming stoichiometry, following the procedure of Droop (1987). Compositions of major elements in the analyzed chromites are listed in Supplementary Appendix A.

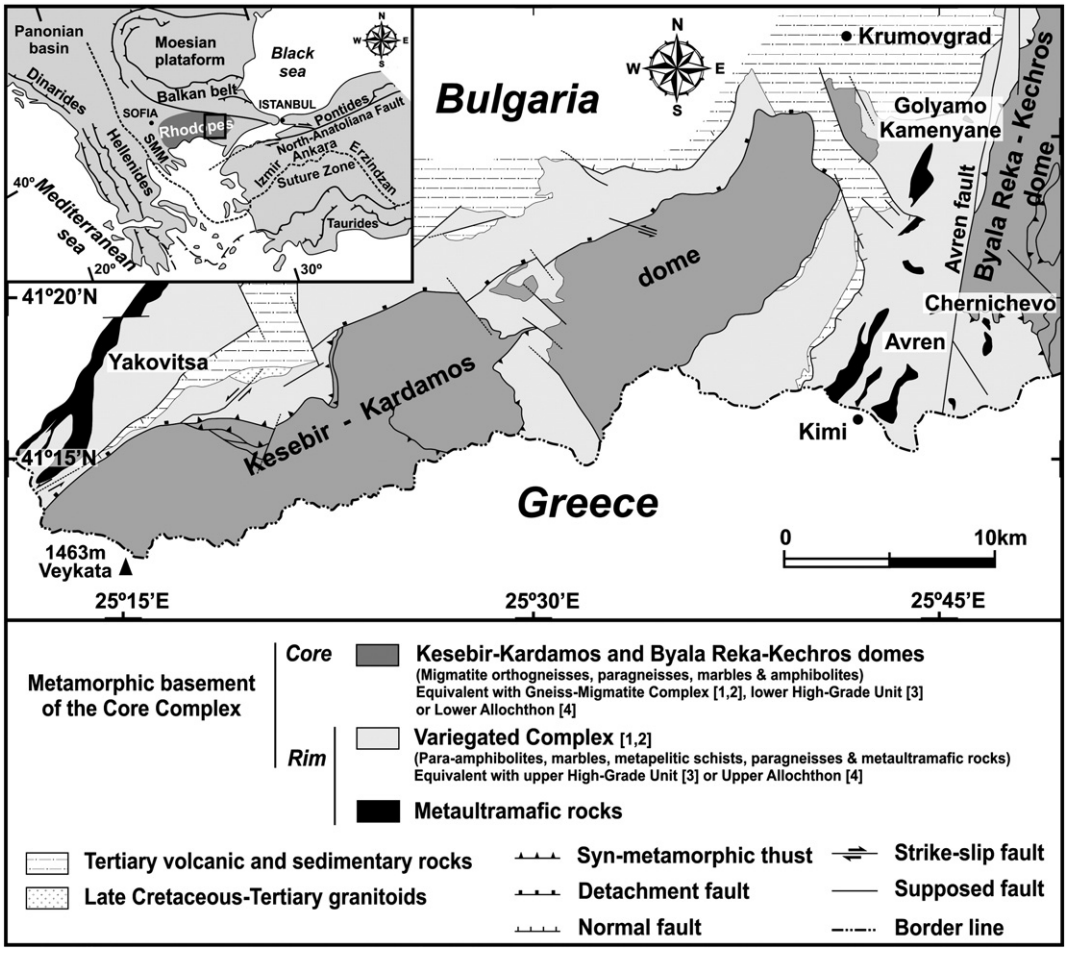

Fig. 1. Simplified geological map of the Eastern Rhodope (modified from Bonev, 2006) showing the localization of the ultramafic massifs hosting the chromitite bodies investigated in this work. Equivalence keys: 1 (Kozhoukharov et al., 1988), 2 (Haydoutov et al., 2001), 3 (Bonev, 2006), and 4 (Janák et al., 2011). Legends are in all cases inset in the figures.

The minor- (detected by EMPA) and trace- (detected only by LA-ICP-MS) element compositions of chromite were determined using a New Wave UP 266 laser system connected to an Agilent 7500cs ICP-MS in the Geochemical Analysis Unit, CCFS/GEMOC, Macquarie University, Sydney. For this study, the chromite analysis focused on the following masses: ^{45}Sc,^{47}Ti, ^{51}V, ^{55}Mn, ^{59}Co, ^{60}Ni, ^{66}Zn, and ^{71}Ga. The isotopes ^{29}Si and ^{42}Ca were monitored to check for the presence of silicate inclusions.

The analyses were conducted using a ~30–55 μm beam diameter, 5 Hz frequency, and 0.032–0.105 mJ/pulse power, during 180 s analysis (60 s for the gas blank and 120 s on the chromite). A setup with small beam diameter (~30 μm) and high power density (3.41–7.65 J/cm^2) was used during the measurement of the small zones free of silicates in porous chromite and thin rims of zoned and partly altered chromite.

The data obtained during ablation runs were processed using the GLITTER software (Griffin et al., 2009). The instrument was calibrated against the NIST 610 silicate glass (National Institute Standards and Technology, Gaithersburg, USA) (Norman et al., 1996). Aluminum values obtained by electron microprobe were used as the internal standard. The basaltic glass BCR-2g (Norman et al., 1996; Gao et al., 2002) and the in-house secondary standard chromite LCR-1 (Lace mine, South Africa; Locmelis et al., 2011) were analyzed as unknowns during each analytical run to check the accuracy and precision of the analyses. The results obtained during the analyses of these two standards display very good reproducibility (3%–8%) for most trace elements (Supplementary Appendix B). All laser ablation data including element concentration, 1-sigma errors and detection limits are presented in Supplementary Appendix C.

4. Results

4.1. Major elements

Our new electron microprobe data (Table 2 and Supplementary Appendix A) for the chromites of Golyamo Kamenyane are consistent with the results of Gervilla et al. (2012), showing that the partly altered chromite of semi-massive chromitites contains apparently unaltered high-Al cores with Cr# [Cr/(Cr + Al) atomic ratio] = 0.52–0.60, Mg# [Mg/(Mg + Fe^{2+}) atomic ratio] = 0.59–0.71 and Fe^{3+}/(Fe^{3+} + Fe^{2+}) = 0–0.30 (Figs. 3a–b and 4a). These cores are surrounded by irregular rims of porous chromite with higher values of Cr# (0.57–0.91), lower Mg# (0.44–0.68) and almost identical Fe^{3+}/(Fe^{3+} + Fe^{2+}) (0–0.28) (Figs. 3a–b and 4a). Grains of porous chromite have lower Mg# (0.35–0.48) but higher Cr_2O_3 (Cr# = 0.91–0.96) and Fe^{3+}/(Fe^{3+} + Fe^{2+}) (0.21–0.53) (Figs. 3a–b and 4a). Non-porous chromite shows Cr# = 0.96–0.99, Mg# = 0.16–0.32 and Fe^{3+}/(Fe^{3+} + Fe^{2+}) = 0.55–0.66 (Figs. 3a–b and 4a). Zoned chromites have cores with Cr# = 0.62–0.69, Mg# = 0.49–0.57 and Fe^{3+}/(Fe^{3+} + Fe^{2+}) = 0.10–0.34, surrounded by non-porous rims with lower Al_2O_3 (Cr# = 0.83–0.99) and Mg# (0.20–0.36) and higher Fe^{3+}/(Fe^{3+} + Fe^{2+}) (0.49–0.63) (Figs. 3a–b and 4a).

Like the chromitites of Golyamo Kamenyane, the other metamorphosed chromitites of the Rhodope show an overall trend of decreasing Al_2O_3 and MgO and increasing Fe^{3+}/(Fe^{3+} + Fe^{2+}) from partly altered chromite to porous and non-porous chromite (Figs. 3a–h and 4a–d). In the semi-massive samples from the small body of Chernichevo, in which only partly altered chromite is preserved (Table 2), the high-Al

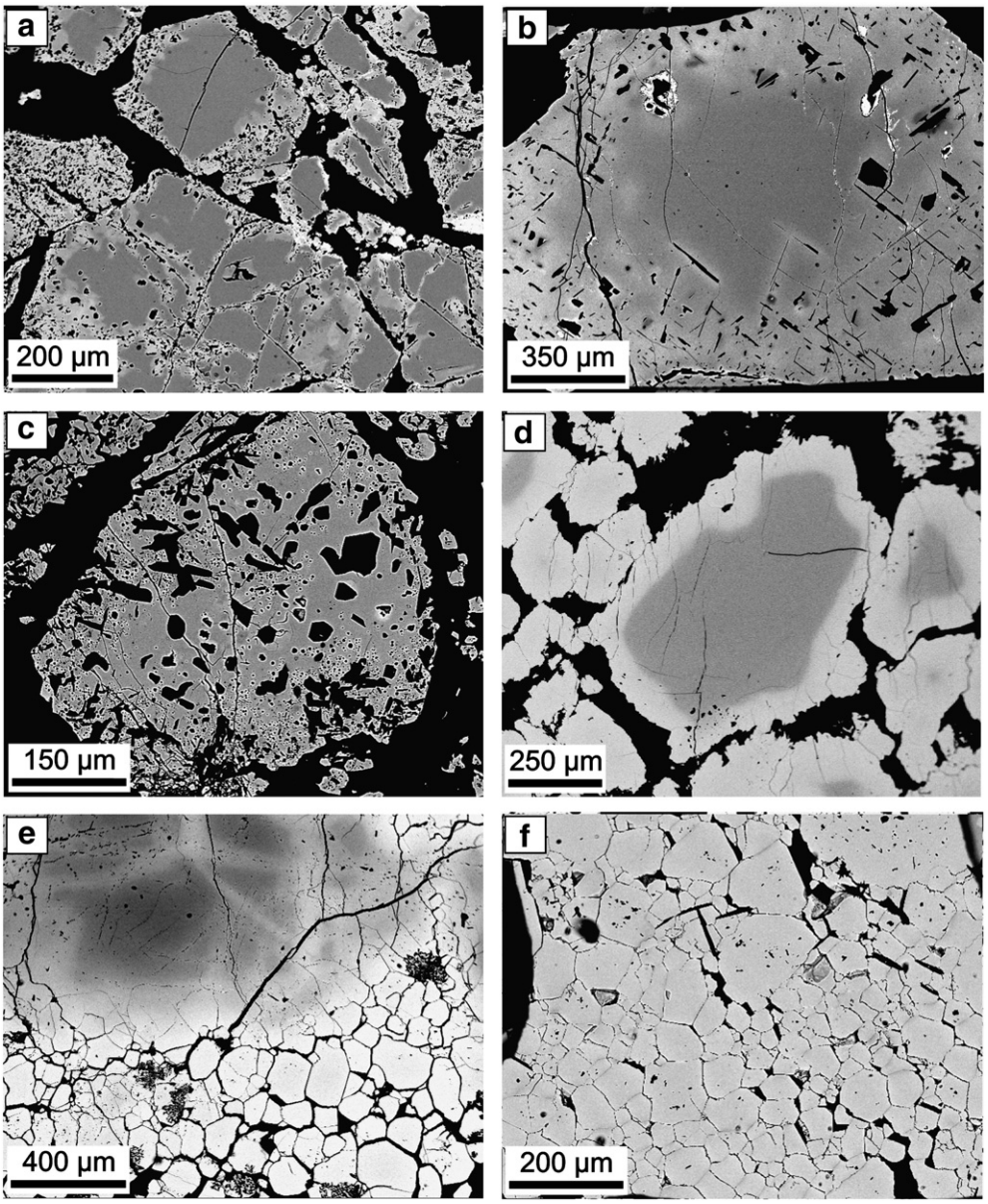

Fig. 2. Back Scattered Electron images of the different microstructural types of chromite that metamorphism has produced in the studied Rhodopean chromitites. Partly altered chromite with (a) thin porous rims from Golyamo Kamenyane and with (b) thick porous rims from Yakovitsa, (c) porous chromite from Golyamo Kamenyane, zoned chromite from Yakovitsa (d) and from Avren (e), and (f) non-porous chromite from Golyamo Kamenyane.

cores (Cr# = 0.55, Mg# = 0.59) show rims of porous chromite with higher Cr# (0.58–0.65) and lower Mg# (0.51–0.57), while $Fe^{3+}/(Fe^{3+} + Fe^{2+})$ (0.27–0.32) remains almost constant (Table 2, Figs. 3c–d and 4b).

In Yakovitsa the high-Cr cores of partly altered chromites from massive and semi-massive chromitites show higher Cr# (0.71–0.78) and Mg# (0.59–0.69) than those of disseminated chromitites (Cr# = 0.60–0.83, Mg# = 0.40–0.65) in smaller bodies (Table 2, Figs. 3e–f and 4c). Cores of grains in samples from massive and semi-massive chromitites are surrounded by rims of porous chromite with similar Cr# (0.78–0.97), but higher Mg# (0.45–0.66) and lower $Fe^{3+}/(Fe^{3+} + Fe^{2+})$ (0.18–0.43) than rims of porous chromite in disseminated chromitites (Cr# = 0.78–0.98, Mg# = 0.29–0.46, $Fe^{3+}/(Fe^{3+} + Fe^{2+})$ = 0.31–0.50) from smaller bodies (Table 2, Figs. 3e–f and 4c). Zoned chromites preserved in disseminated samples from the smallest chromitite body (<20 cm thickness) have cores with similar Cr# (0.68–0.73) but lower Mg# (0.38–0.42) and $Fe^{3+}/(Fe^{3+} + Fe^{2+})$ (0.08–0.17) than the cores of partly altered chromite. These cores are surrounded by rims of non-porous chromite with the highest observed Cr# (0.91–0.98) and $Fe^{3+}/(Fe^{3+} + Fe^{2+})$ (0.46–0.61), and the lowest Mg# (0.16–0.27) (Table 2, Figs. 3e–f and 4c).

Zoned chromites in the chromitites from Avren have high-Cr cores with variable Cr# (0.84–0.93) and Mg# (0.35–0.46), but weakly variable $Fe^{3+}/(Fe^{3+} + Fe^{2+})$ (0.19–0.31); these are surrounded by rims of non-porous chromite with higher Cr# (0.93–0.98) and $Fe^{3+}/(Fe^{3+} + Fe^{2+})$ (0.50–0.67), and lower Mg# (0.08–0.35) (Table 2, Figs. 3g–h and 4d).

4.1.1. Minor and trace elements

Minor- and trace-element compositions of the chromitites are presented in Supplementary Appendix C. Fig. 5 shows spidergrams with the compositions of analyzed chromites normalized to the composition of chromite from East Pacific Rise MORB plotted following the

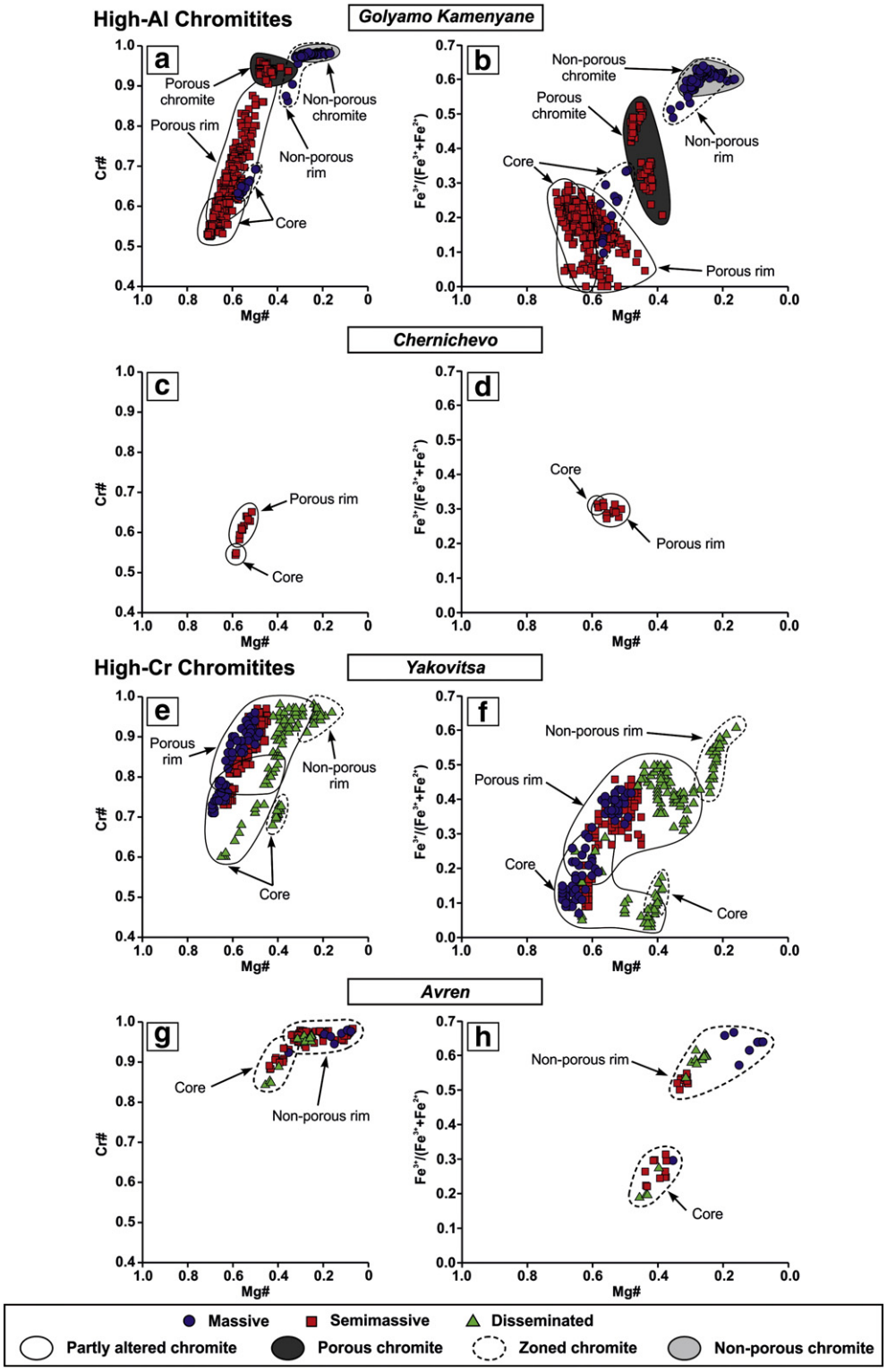

Fig. 3. Compositional variations of chromites from the studied chromitites in terms of Mg# [Mg/(Mg + Fe^{2+}) atomic ratio] versus Cr# [Cr/(Cr + Al) atomic ratio] and $Fe^{3+}/(Fe^{3+} + Fe^{2+})$. Legend is inset in the figure.

order of elements suggested by Pagé and Barnes (2009). We use the composition of this chromite as a basis for normalization because repeated laser ablation analyses by these authors show that it has a homogenous and uniform distribution of minor and trace elements.

Partly altered chromites in the semi-massive chromitites from Golyamo Kamenyane have cores and porous rims characterized by "flat" patterns with strong negative anomalies in Ti and Sc relative to MORB (Fig. 5a–b). In contrast, grains of porous chromite with lower Al_2O_3 and MgO are more depleted in Ga, Ni, V and Sc, but slightly enriched in Ti, Zn, Co and Mn relative to the cores and porous rims of partly altered chromite (Fig. 5c). In some grains of porous chromite there is a strong M-shaped positive anomaly in the segment Zn–Co–Mn (hereafter ZCM-anomaly; Fig. 5c). Grains of porous chromite have cores with lower contents of Ti, Zn, Co and Mn than

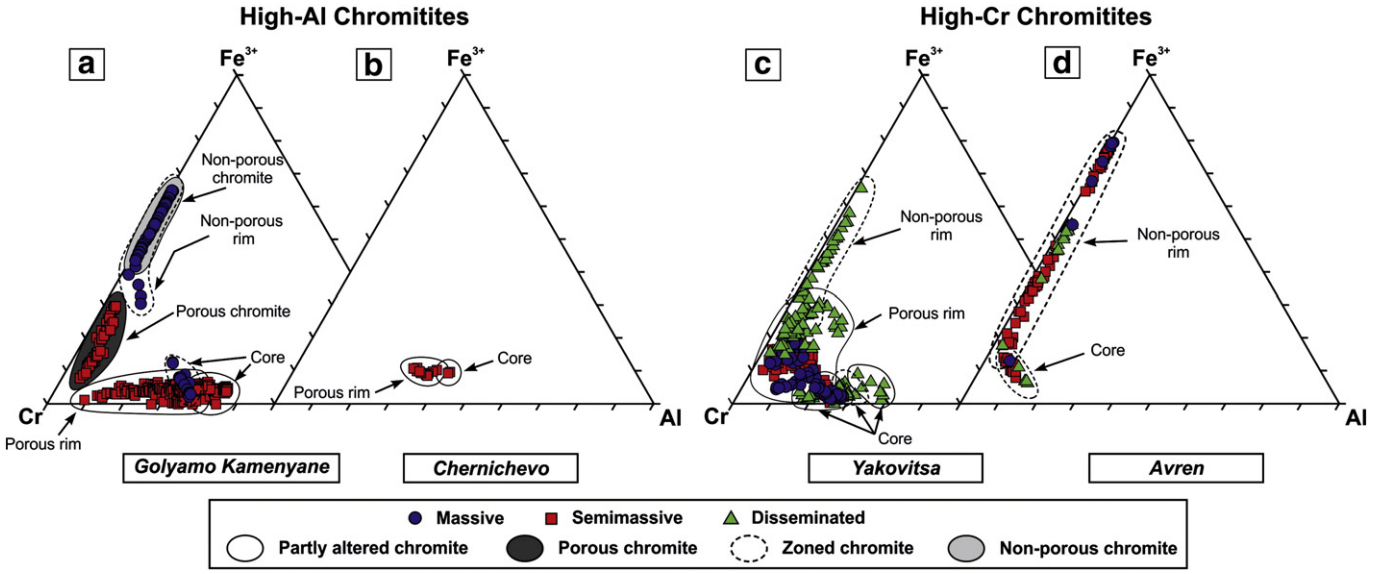

Fig. 4. Variations of Al^{3+}, Cr^{3+} and Fe^{3+} in chromites from the studied chromitites. Legend is inset in the figure.

their outermost parts, but with higher contents of V and similar contents of Ga, Ni, and Sc. The cores of zoned chromite grains in massive chromitites also show strong depletion in Sc, Ni, Ga and Ti, while the enrichment in the segment Zn–Co–Mn does not define a ZCM-anomaly (Fig. 5d). The latter pattern is distinctly different from that of non-porous chromite (also found surrounding these cores) which has lower Al_2O_3 but higher Ga, Ti, Ni and Sc, and the ZCM-anomaly (Fig. 5e–f).

Partly altered chromites from Chernichevo have cores and rims showing almost identical flat trace-element patterns. Relative to MORB chromite, the chromitites from Chernichevo show a distinct

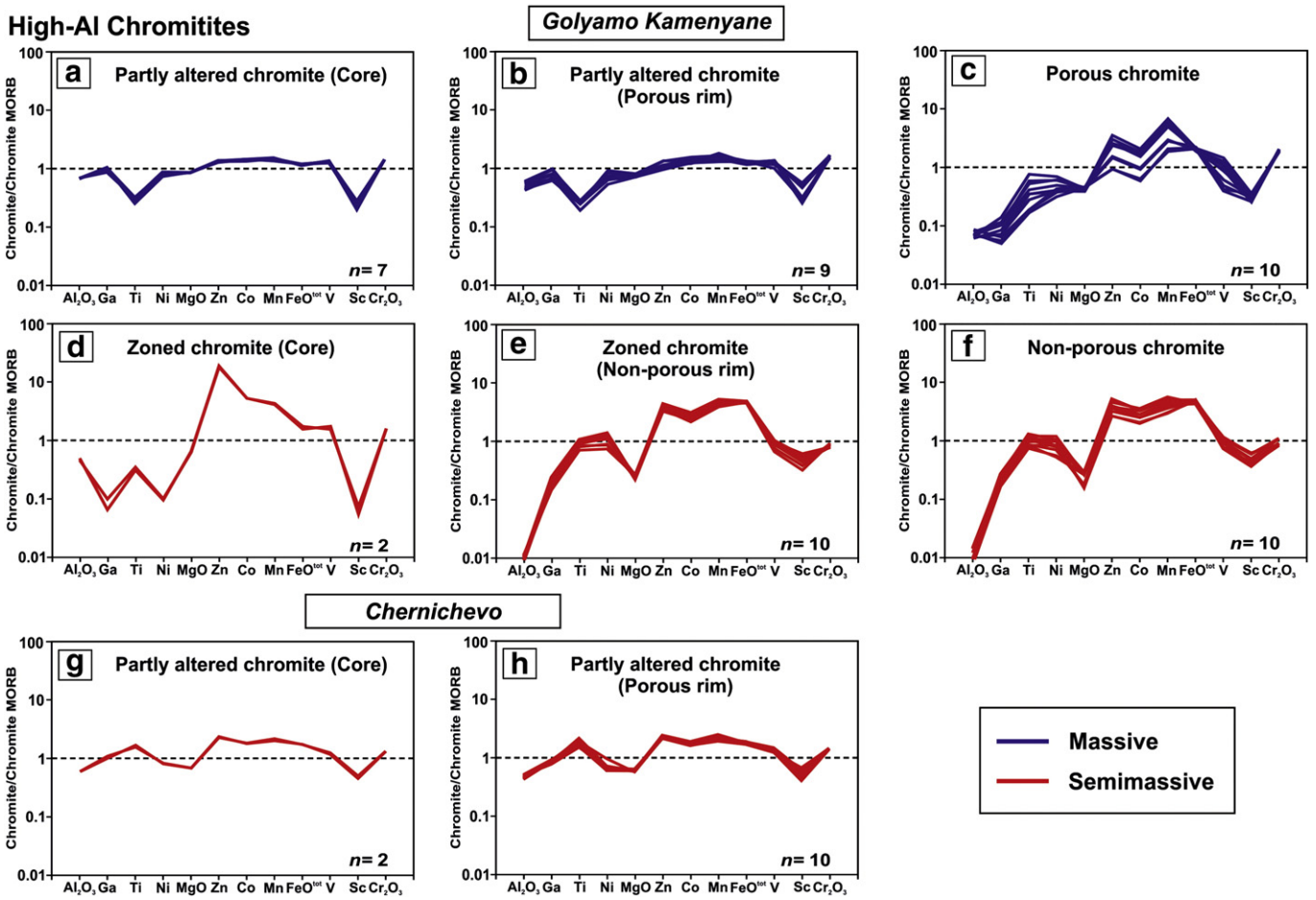

Fig. 5. Spidergrams showing the composition (major, minor and trace elements) of the different microstructural types of chromite from the studied Rhodopean chromitites. The analyzed compositions are normalized to the composition of chromite from MORB (Pagé and Barnes, 2009). Legend is inset in the figure.

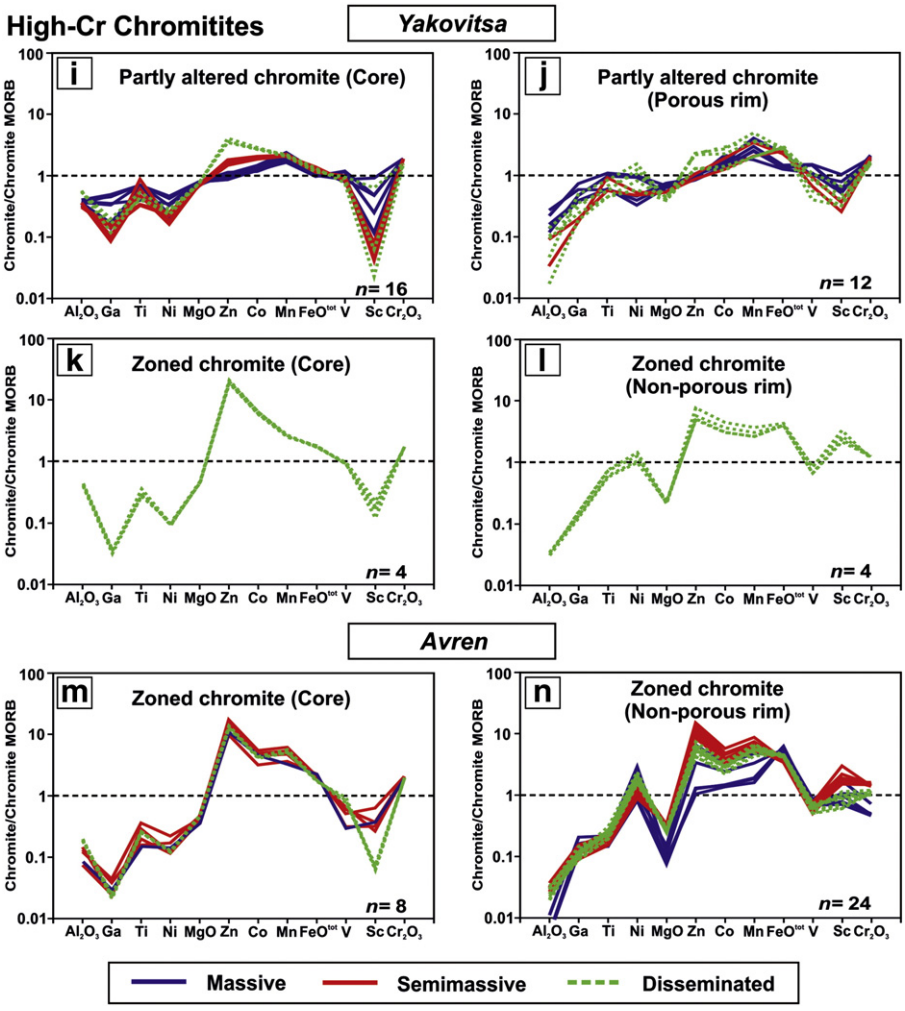

Fig. 5 (*continued*).

enrichment in Ti coupled with a less marked ZCM-anomaly and depletion in Sc (Fig. 5g–h).

In the Yakovitsa occurrence, the high-Cr cores of partly altered chromites show positive slopes in their patterns, produced by depletion in Ga, Ti, Ni and Sc, and enrichment in Zn, Co and Mn relative to MORB chromite (Fig. 5i). The first segment of the pattern is characterized by enrichment in Ti relative to Ga and Ni. The cores of partly altered chromite from the massive chromitites have higher contents of Ga, Ti, Ni and Sc and lower Zn and Co than the cores of chromites from smaller bodies of disseminated chromitite (Fig. 5i). The rims of porous chromite surrounding these cores show substantially different patterns, with slightly higher contents of Ga, Ni, Mn and Sc but overall lower Al_2O_3 and V (Fig. 5j). Zoned chromites in the disseminated chromitites have cores with patterns almost identical to the cores of zoned chromites of the Golyamo Kamenyane chromitites (Fig. 5d and k). These cores are depleted in Ga, Ti, Ni and Sc, and enriched in Zn, Co and Mn relative to chromite from MORB, but are enriched in Ti relative to Ga and Ni and show a pronounced positive anomaly in Zn (Fig. 5k). However, the rims surrounding these cores have much higher contents of Sc (producing a positive anomaly) as well as Ga, Ti and Ni, but lower Zn, Co and Mn (Fig. 5l).

The zoned chromites of Avren show high-Cr cores with trace-element patterns somewhat similar to that of the cores of zoned chromites from Golyamo Kamenyane and Yakovitsa (Fig. 5d, k and m). In contrast, the rims of non-porous chromite show a gentler slope in the segment Ga–Ti, coupled with a marked positive anomaly in Ni and a negative one in MgO (Fig. 5n). These patterns also show the typical ZCM-anomaly and enrichment in Sc relative to MORB chromite, like the similar rims from Yakovitsa (Fig. 5l and n).

5. Discussion

5.1. Metamorphism of the chromitites of the Eastern Rhodope

Gervilla et al. (2012) explained the origin of the different microstructures of chromitites in the Golyamo Kamenyane massif as the consequence of a two-stage process involving the infiltration of fluids during the retrograde metamorphic evolution of the Rhodope Metamorphic Core Complex.

During the first stage, the hydration of olivine from the host dunite released significant amounts of H_2, which contributed to a much lower fO_2 by its reaction with O_2 to form water (e.g., Bach et al., 2006). In the chromitite bodies, the infiltration of these reducing fluids probably promoted the reaction of primary chromite with matrix olivine, giving rise to chlorite and to secondary chromite residually enriched in Cr and Fe^{2+} by loss of Al_2O_3 and MgO to the chlorite (Fig. 6). This metamorphic event is well recorded in the partly altered chromites of Golyamo Kamenyane, which show a decrease in Mg# (0.59–0.71), and an increase in Cr# (0.52–0.60), but nearly unchanged $Fe^{3+}/(Fe^{3+} + Fe^{2+})$ (0–0.30), from core to rim (Mg# = 0.44–0.68,

Cr# = 0.57–0.91 in the porous rim; Fig. 3a–b). This replacement involves mass loss from chromite grains without changes in their size, resulting in the formation of pores (i.e. *porous chromite*), which may be filled by the chlorite produced during the reaction (Figs. 2a–c and 6). Thermodynamic modeling by Gervilla et al. (2012) suggests that this reaction took place during cooling of the rocks through an interval from ~700 to ~450 °C.

Once olivine was exhausted in the host dunite and the chromitite, the fO_2 shifted progressively to higher values (i.e., more oxidizing conditions; Alt and Shanks, 1998; Allen and Seyfried, 2003; Bach et al., 2004; Alt et al., 2007). This variation in fO_2 changed the conditions of chromite alteration, producing a different type of metamorphic chromite. These fluids with progressively higher fO_2 infiltrated the network of pores in the Cr- and Fe^{2+}-rich porous chromite, depositing magnetite while dissolving chlorite in the pores, thus promoting the diffusion of Fe^{2+} and Fe^{3+} into chromite and eliminating the porous textures to produce a non-porous chromite significantly enriched in Fe^{3+} (i.e. ferrian chromite; Fig. 6). Fe^{2+} and Fe^{3+} can easily diffuse through the porous rims of the chromite grains but diffusion is slower in the unaltered, non-porous core, which results in the formation of *zoned chromite* (Fig. 2d–e). This explains why in the zoned chromites of Golyamo Kamenyane there is an increase in $Fe^{3+}/(Fe^{3+} + Fe^{2+})$ (0.10–0.34) and Cr# (0.62–0.69), and a decrease in Mg# (0.49–0.57), from core to rim ($Fe^{3+}/(Fe^{3+} + Fe^{2+}) = 0.49–0.63$, Cr# = 0.83–0.99, Mg# = 0.20–0.36, in the non-porous rim; Fig. 3a–b). During this second stage, which might also involve the transformation of some chlorite to antigorite, the amount of Fe^{2+} and Fe^{3+} supplied by the infiltrating fluids might exceed the volume of pre-existing pores, promoting the coarsening of chromite to produce *non-porous chromite* with mosaic or polygonal textures (Figs. 2f and 6).

Phase relations in the system $(Fe^{2+}, Mg)Cr_2O_4$–$(Fe^{2+}, Mg)Fe^{3+}{}_2O_4$–$(Fe^{2+}, Mg)Al_2O_4$ suggest that the studied non-porous chromite could form at temperatures < 600 °C (Sack and Ghiorso, 1991; Gervilla et al., 2012), overlapping the formation of Fe^{2+}-rich chromite. According to Gervilla et al. (2012), in the Golyamo Kamenyane massif both stages in the alteration of chromite took place as the rocks cooled from ~700 to ~450 °C along the eclogite- to amphibolite-facies retrograde metamorphic pathway (Mposkos and Krohe, 2000, 2006; Mposkos, 2002; Haydoutov et al., 2004) associated with the exhumation of the *allochthonous rim* of the Eastern Rhodope.

The microstructures and chemical variations of chromite from the other metamorphosed chromitites of the Eastern Rhodope can also be interpreted in terms of the two-stage process described for the chromites of Golyamo Kamenyane (Gervilla et al., 2012) (Fig. 6). Evidence for the first stage is preserved as Cr- and Fe^{2+}-rich porous rims surrounding the cores of partly altered chromite in the Chernichevo (high-Al chromites) and Yakovitsa (high-Cr chromites). In the latter the reaction of high-Cr chromite with the olivine matrix had produced Cr-rich clinochlore, similar to that replacing high-Cr chromites in the nearby Dobromirtsi Ultramafic Massif (González Jiménez et al., 2009) and metamorphosed chromitites elsewhere (e.g., Jan and Windley, 1990; Merlini et al., 2009; Mukherjee et al., 2010). In chromitites from Chernichevo and Yakovitsa, the oxidizing second stage did not completely erase the pores, but only contributed to increase the magnetite component in the Fe^{2+}-rich porous chromite (Table 2; Figs. 3c–f and 6). In contrast, in some of the disseminated chromitites in the smallest chromitite bodies in Yakovitsa and Avren, the oxidizing fluids were able to precipitate enough material in the cavities of porous chromite to produce zoned and non-porous chromite (Table 2; Figs. 3e–h and 6).

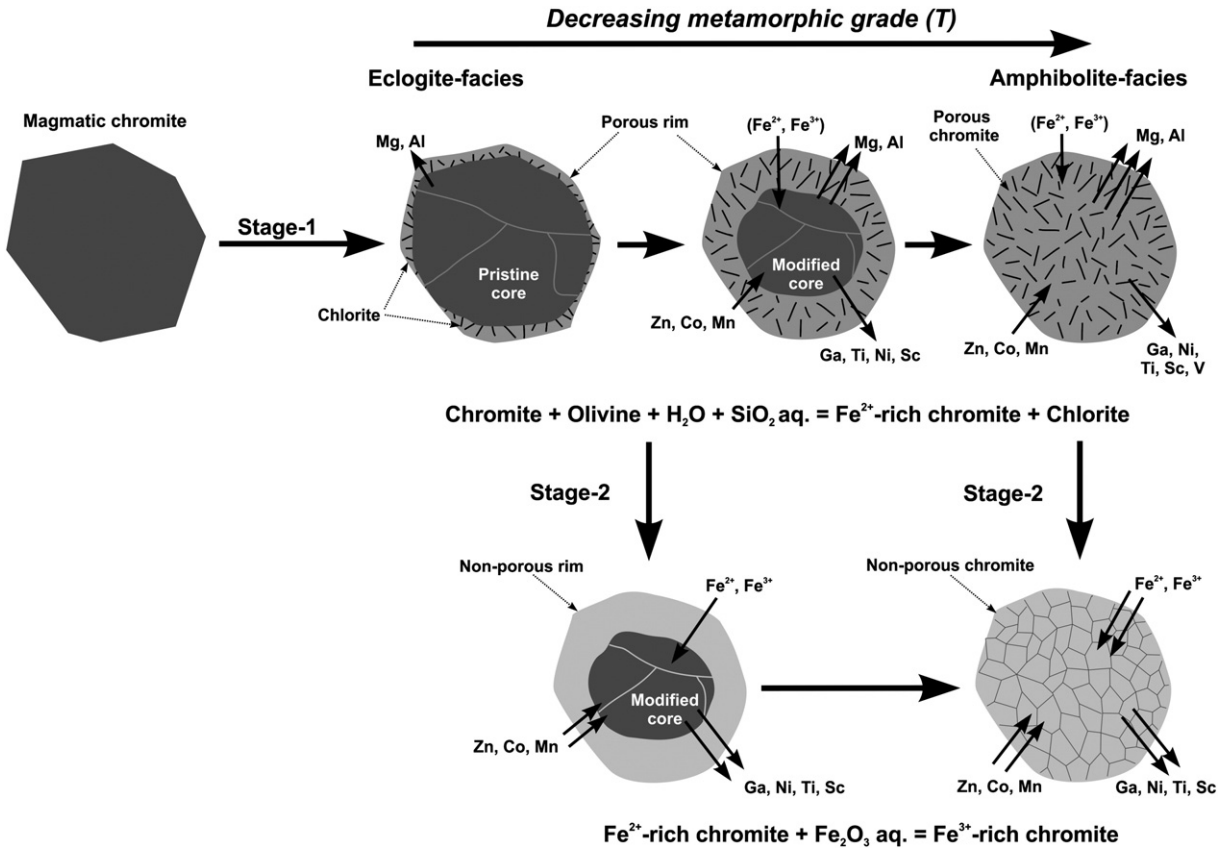

Fig. 6. Schematic illustration of microstructural and chemical (major, minor and trace elements) changes in chromites, showed as two-stage processes of alteration during the retrograde evolution of chromitites from the Eastern Rhodope. The extent of reaction is noted in the figure with number of arrows.

The preservation of porous chromite rims and/or their obliteration by the formation of rims of non-porous chromite is directly associated with the ability of the infiltrating fluids to penetrate the chromite. The effectiveness of the altering fluids would depend on (1) their ability to penetrate chromite, mainly controlled by the chromite/silicate ratio and the presence of secondary permeability such as fractures; (2) the availability of enough fluid to allow higher rates of interaction between the infiltrating fluids and chromite. The fact that some grains only show porous textures whereas others have compositionally-distinct porous rims of variable thickness (Fig. 2a–c; Table 2) shows that the alteration process did not operate in the same way in different parts of individual chromitite bodies. Zoned and non-porous chromites are mostly found in sheared chromitites collected from faults cutting the bodies. This clearly indicates that a strong fracture network and associated deformation facilitated the circulation of fluids, helping the nucleation and/or dynamic recrystallization of ferrian chromite (Satsukawa et al., 2014).

Gervilla et al. (2012) noted that in the Golyamo Kamenyane massif chromitites are cut by veins of anthopyllite, whereas veins filled by asbestos and talc cut chromitites in the Avren massif. In this scenario, shear zones probably acted as channels for focused migration of the oxidizing fluids producing the nearly complete replacement of the pre-existing porous chromite by Fe^{3+}-rich non-porous chromite. This focused infiltration of the oxidizing fluids along the shear zones would prevent the obliteration of the porous textures in the rest of the massif (e.g., areas outside the shear zones). An almost complete replacement of porous chromite by non-porous chromite in these shear zones can explain why we do not observe grains with inner rims of porous chromite and outer rims of non-porous chromite in some of the chromitites from Golyamo Kamenyane, Yakovitsa and Avren (Fig. 2). This is consistent with the observations that veins of anthophyllite cut some chromitites in Golyamo Kamenyane (Gervilla et al., 2012) and veins of asbestos and talc cut some at Avren (Kolkovski et al., 2003).

5.2. Trace-element fingerprints of metamorphism in the cores of partly altered chromites

The high-Cr cores of partly altered chromite in massive and semi-massive chromitite bodies (>40 cm thickness) from Yakovitsa have higher Mg# (0.59–0.69) than chromite in thinner bodies (20–30 cm thickness) made up only of disseminated chromitite (Mg# = 0.40–0.65) (Table 2; Fig. 3e–f). This trend of enrichment of Fe^{2+} (i.e., higher contents in cores of chromite from disseminated samples relative to those from massive chromitites) is somewhat similar to that described in grains of chromite from unmetamorphosed massive and disseminated chromitites in ophiolites elsewhere (e.g. Leblanc and Nicolas, 1992). It is usually attributed to the diffusion of Fe^{2+} and Mg^{2+} between chromite and olivine at high temperatures (1,000–900 °C) during post-magmatic cooling (Table 1; Barnes, 2000; Kamenetsky et al., 2001; Rollinson et al., 2002). However, Candia and Gaspar (1997) have reported similar trends in chromite grains that have re-equilibrated with the host olivine matrix during metamorphism at 750–700 °C and $P_{H_2O} = P_{tot}$. These conditions are similar to those of the eclogite-facies metamorphism that affected the chromitites of the Eastern Rhodope (775–750 °C; Mposkos and Krohe, 2000, 2006; Mposkos, 2002; Gervilla et al., 2012). The microstructures and the variations of Mg#, Cr# and $Fe^{3+}/(Fe^{3+} + Fe^{2+})$ in the cores of partly altered chromites from Yakovitsa do not allow discrimination between the two processes.

To further assess the effects of metamorphism on the cores of partly altered chromites from Yakovitsa we have compared their minor- and trace-elements patterns with the composition of high-Cr chromites from an unmetamorphosed chromite body of similar size. The chromitite dike selected is from the locality of Dyne in the New Caledonia Ophiolite and has cross-section dimensions of 8.5 × 0.5 m (Leblanc et al., 1980; Cassard et al., 1981; Fig. 7a–b). The chromite grains from Dyne have experienced extensive sub-solidus $Mg^{2+} \leftrightarrow Fe^{2+}$ exchange with olivine during cooling; it is recorded by the decrease of Mg# at constant Cr# in the chromites with lower chromite/silicate ratios (Fig. 7b). The patterns of minor- and trace elements in the unmetamorphosed chromite grains of Dyne are almost identical to those of high-Cr chromite in massive chromitites from unmetamorphosed ophiolites (Fig. 7a) such as Thetford Mines (Pagé and Barnes, 2009) and Eastern Cuba (González-Jiménez et al., 2013, 2014), which make them very useful to our propose.

The cores of partly altered chromites from Yakovitsa have patterns distinctly different from the unmetamorphosed chromites of Dyne, being more depleted in Ga and Sc, and enriched in Zn, Co and Mn; the concentrations of Ti can be higher or lower (Fig. 5i and 7a). Despite these notable differences, both the unmetamorphosed chromites from Dyne and the cores of partly altered chromites from Yakovitsa show a similar negative correlation between Ga and Zn + Co + Mn as Mg# decreases at lower chromite/silicate ratio (Fig. 7b–c). However, in the unmetamorphosed chromites of Dyne the decrease of Mg# occurs at constant Cr#, whereas the decrease of Mg# in the cores of partly altered chromites from Yakovitsa is associated with an increase of Cr#, driven by the formation of porous rims and the sequestering of Al and Mg into the metamorphic chlorite. Gallium, like Al, is a trivalent cation that does not enter the olivine lattice but can be taken up by chlorite (up to 31 ppm in our samples; Table 1). This suggests that the negative correlation of Ga vs Zn + Co + Mn observed in Fig. 7c could be a consequence of the metamorphism rather than of subsolidus re-equilibration between chromite and olivine during cooling.

Gallium, Ni, Sc and Ti decrease from the inner to the outer part in the cores of partly altered chromite at a relatively constant Mg# (Fig. 8a–d), but these have complex relationship to $Fe^{3+}/(Fe^{3+} + Fe^{2+})$ (Fig. 8e–h). In the cores of partly altered chromite of massive chromitites there are no correlations among Ga, Ni, Sc, Ti and $Fe^{3+}/(Fe^{3+} + Fe^{2+})$, whereas the latter increase from the inner to the outer part in the cores of partly altered chromites of semi-massive and disseminated chromitites (Fig. 8e–h). This suggests that the diffusion of minor- and trace elements from core to Fe^{2+}-rich porous rims in partly altered chromites results from the re-ordering of Fe^{2+} and Fe^{3+} into octahedral and tetrahedral sites (Fig. 1 in Sack and Ghiorso, 1991), which promoted the entrance of Ni^{2+} into octahedral positions and Ga^{3+}, Sc^{3+} and Ti^{4+} into the tetrahedral sites. The latter effect, combined with the higher degree of infiltration of fluids into chromitites with lower chromite/silicate ratios, produced thicker rims of Fe^{2+}-rich porous chromite, promoting higher mobilization and enrichment of Ga, Ni, Sc and Ti, from cores to porous rims in partly altered chromites (Figs. 5i–j and 6).

The highest values of Zn, Co and Mn, and very low Mg#, occur in cores of partly altered chromites in disseminated samples (Fig. 8i–k). This may indicate a greater degree of substitution in samples with higher proportions of olivine (González Jiménez et al., 2009). Zinc, Co and Mn, together with Fe^{2+}, can enter the tetrahedral sites vacated by Mg^{2+} sequestered into olivine during cooling and subsolidus re-equilibration between chromite and olivine, as is observed in the unmetamorphosed chromites of Dyne (Table 1; Fig. 7b). However, the coincidence of enrichment in Zn, Co and Mn with stronger depletion in Ga, Sc and Ni (Fig. 7c), and the fact that all of these elements show very distinct correlations with $Fe^{3+}/(Fe^{3+} + Fe^{2+})$ (Fig. 8l–n), suggest a complex interplay of substitutions during the metamorphism. Thus the contents of Mn increase from the inner to the outer parts of the cores in massive samples at constant $Fe^{3+}/(Fe^{3+} + Fe^{2+})$, but are constant as $Fe^{3+}/(Fe^{3+} + Fe^{2+})$ increases in semi-massive and disseminated ones (Fig. 8n). This suggests that in samples with the lowest chromite/silicate ratio, the formation of Fe^{2+}-rich porous chromite promotes the re-ordering of Fe^{2+}, limiting the substitution of Fe^{2+} (in octahedral sites) by Mn^{2+}, Zn and Co (Fig. 6). This can explain why, in these cores of partly altered chromite, Zn and Co decrease with increasing $Fe^{3+}/(Fe^{3+} + Fe^{2+})$ (Fig. 8l–m). Taken together these observations suggest that the positive ZCM-anomaly, coupled with depletion in Ga, Ni and Sc, is a fingerprint of amphibolite-facies metamorphism in the high-Cr cores of partly altered chromites from Yakovitsa. These

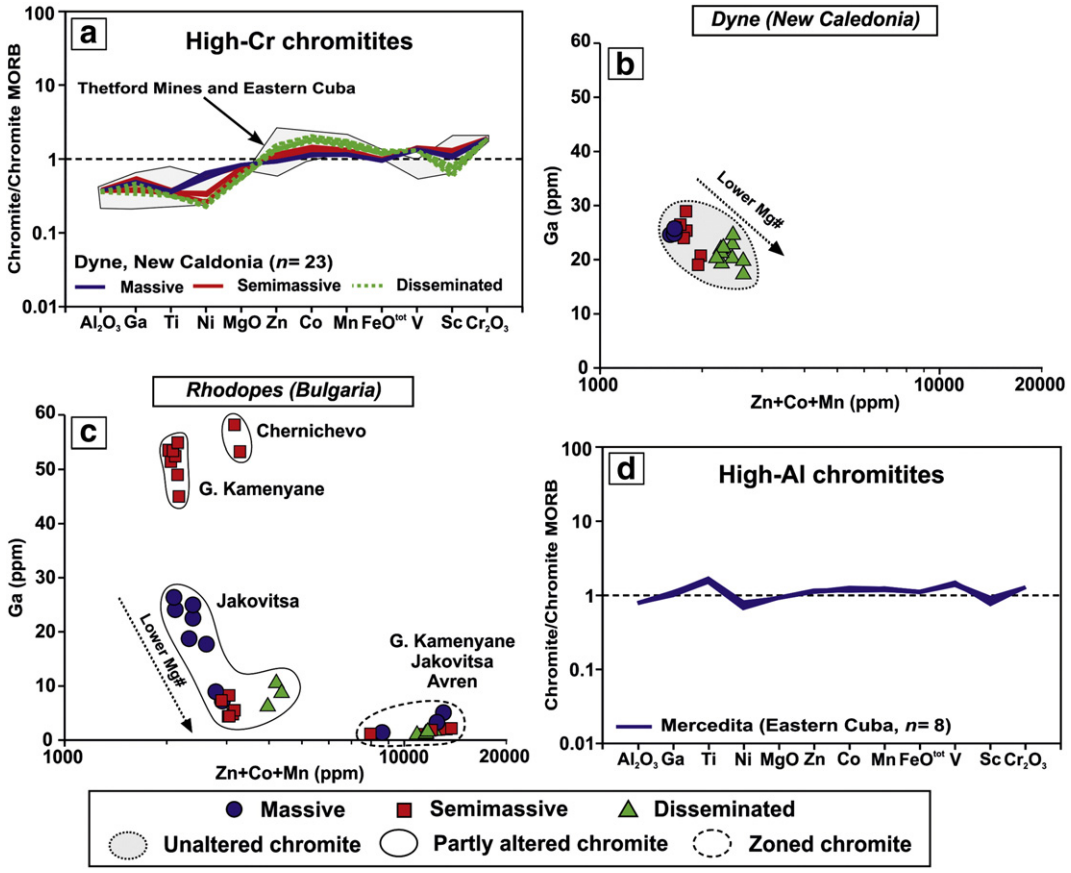

Fig. 7. Spidergrams showing the composition (major, minor and trace elements) of high-Cr chromite in unmetamorphosed massive chromitites from Thetford Mines (Pagé and Barnes, 2009) and Eastern Cuba (González-Jiménez et al., 2013, 2014), and from the chromitite dike of Dyne (New Caledonia) (a). Compositional variation in terms of Zn + Co + Mn (ppm) vs Ga (ppm) of unmetamorphosed chromites from the chromitite dike of Dyne (New Caledonia) (b) and chromite cores from the studied Rhodopean chromitites (c). Spidergrams showing the major, minor and trace elements composition in high-Al chromite from unmetamorphosed massive chromitites from Mercedita (Eastern Cuba) (d). The analyzed compositions are normalized to the composition of MORB chromite (Pagé and Barnes, 2009). Legend is inset in the figure.

chemical variations were produced, or strengthened, by the exchange of cations between these cores and their surrounding porous rims filled with chlorite (Fig. 6).

On the other hand, the cores of partly altered high-Al chromites from Golyamo Kamenyane and Chernichevo show elemental patterns almost identical to their surrounding porous rims (Fig. 5a–b and g–h). This may suggest that either (1) the infiltrating fluids did not substantially modify the trace- and minor elements or (2) an almost complete re-equilibration was reached between the cores and their surrounding rims. The first alternative is supported by the fact that the patterns of those cores are practically identical to the "flat" patterns of high-Al massive chromitites in the unmetamorphosed ophiolites of Eastern Cuba (Fig. 7d). The porous rim of partly altered chromites from Golyamo Kamenyane and Chernichevo are very thin (Fig. 2a), indicating that a limited reaction between cores and infiltrating fluids prevented an extensive exchange of elements (Fig. 6). In contrast, higher fluid/rock ratios promoted higher rates of reaction between the small grains of chromite and infiltrating fluids, resulting in complete replacement by porous chromite in Golyamo Kamenyane (Fig. 6). This can explain why these grains exhibit the ZCM-anomaly coupled with strong depletion in Ga, Ni, Sc and V, as preserved in the modified cores of partly altered chromites from Yakovitsa (Fig. 5c and i).

In the grains of porous chromite from Golyamo Kamenyane there are also complex relationships between the trace elements and $Fe^{3+}/(Fe^{3+} + Fe^{2+})$ (Fig. 8o–v). Thus, during the reaction of primary chromite with olivine in the presence of reducing fluids, Mg^{2+} and Ni^{2+} would be lost from the chromite, while Fe^{2+} was added together with Zn, Co and Mn (Fig. 6). This Fe^{2+}-rich chromite has a normal spinel structure but with fewer available octahedral sites than the pristine chromite (Sack and Ghiorso, 1991), thus explaining their relative depletion in Ga, V and Sc (Fig. 6). Interestingly, the grains of porous chromite exhibit a wider range of Ti and higher Fe^{3+} contents (in octahedral sites) than the porous rims of partly altered chromite grains (Fig. 8v). This suggests that the porous chromite grains had re-equilibrated to a greater extent with infiltrating fluids rich in Fe^{3+}, added during the second stage of alteration. These fluids did not contribute to eliminating the pores in the porous chromite but promoted the re-ordering of octahedral sites in the chromite lattice and thus, facilitated the incorporation of Ti^{4+} (Fig. 6).

5.3. Minor- and trace elements and the precipitation of ferrian chromite

As noted above, the second stage of alteration during the metamorphism of the Rhodopean chromitites involved the infiltration of oxidizing fluids through the pores of the porous chromite, to produce non-porous rims or grains of ferrian chromite (Gervilla et al., 2012).

The non-porous rims of ferrian chromite on the zoned chromites from the high-Cr (Yakovitsa and Avren) and high-Al chromitites (Golyamo Kamenyane) show very similar patterns of minor- and trace elements (Fig. 5e, l and n). These profiles are identical to that observed in non-porous ferrian chromite in the Golyamo Kamenyane chromitites (Fig. 5f), which suggests their alteration by a common fluid that has obliterated the geochemical fingerprint of the pre-existing chromite regardless of its original composition. Interestingly, the cores of the zoned chromites show patterns with very similar shapes, although very different to those of their surrounding rims. Overall, these cores are more

depleted in Ga, Ni and Sc and more enriched in Zn and Co (Fig. 5d, k and m) than the non-porous ferrian chromite. The profiles of these cores of zoned chromites are distinctly different from those of the cores of partly altered chromites within the same chromitite body, indicating how their composition was influenced by reaction with a specific type of rim (i.e. Fe^{2+}-rich and porous vs Fe^{3+}-rich and non-porous). The

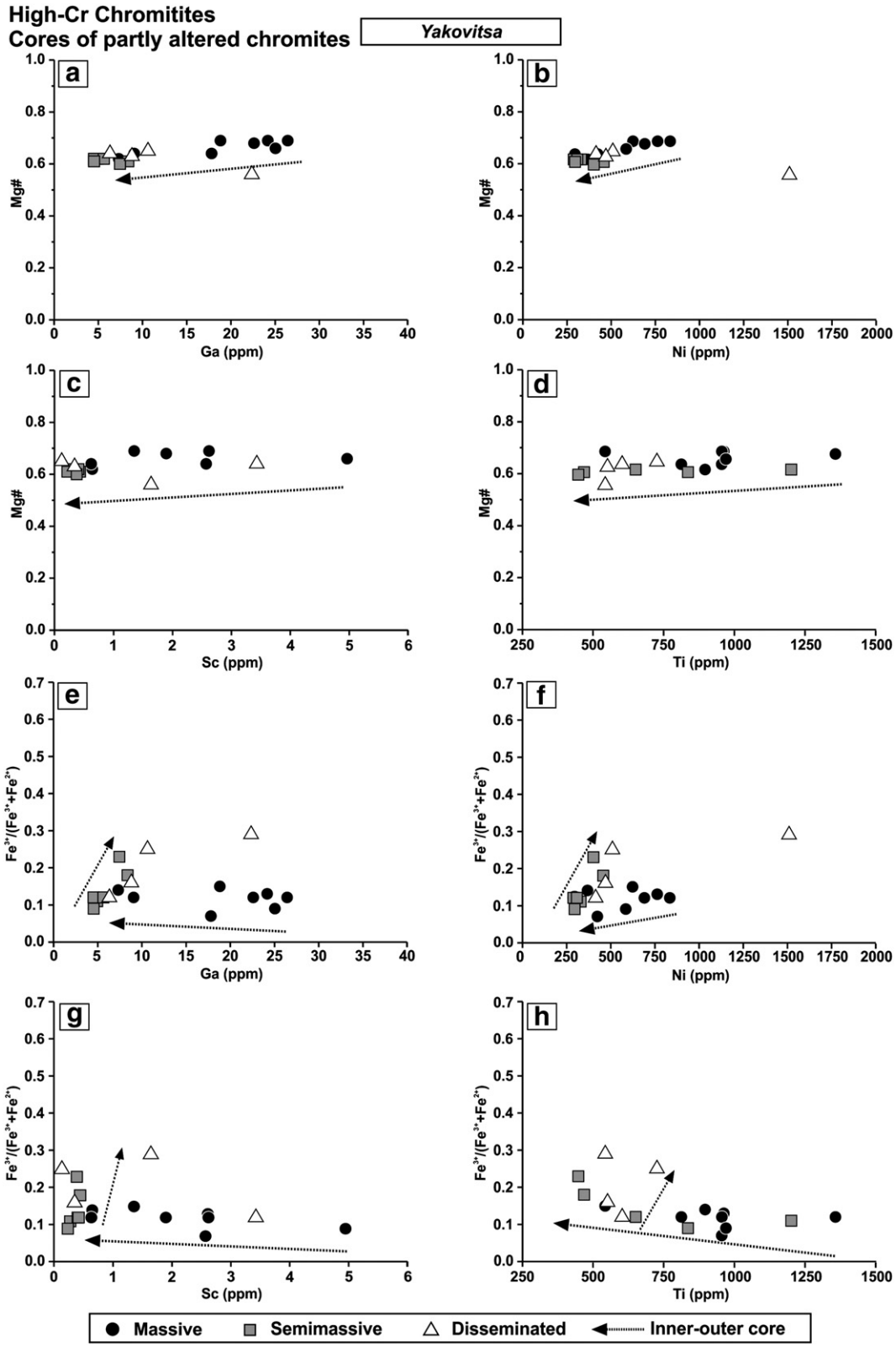

Fig. 8. Compositional variations in the high-Cr cores of partly altered chromite from Yakovitsa in terms of Zn, Co, Mn, Ga, Ni, Sc and Ti (in ppm) versus Mg# [$Mg/(Mg + Fe^{2+})$ atomic ratio] and $Fe^{3+}/(Fe^{3+} + Fe^{2+})$ (a–n). Variations of Ni, Zn, Co, Mn, Ga, V, Sc and Ti contents (in ppm) versus $Fe^{3+}/(Fe^{3+} + Fe^{2+})$ in the porous rims of partly altered chromite and the porous chromite of high-Al chromitites at Golyamo Kamenyane (o–v). Legend is inset in the figure.

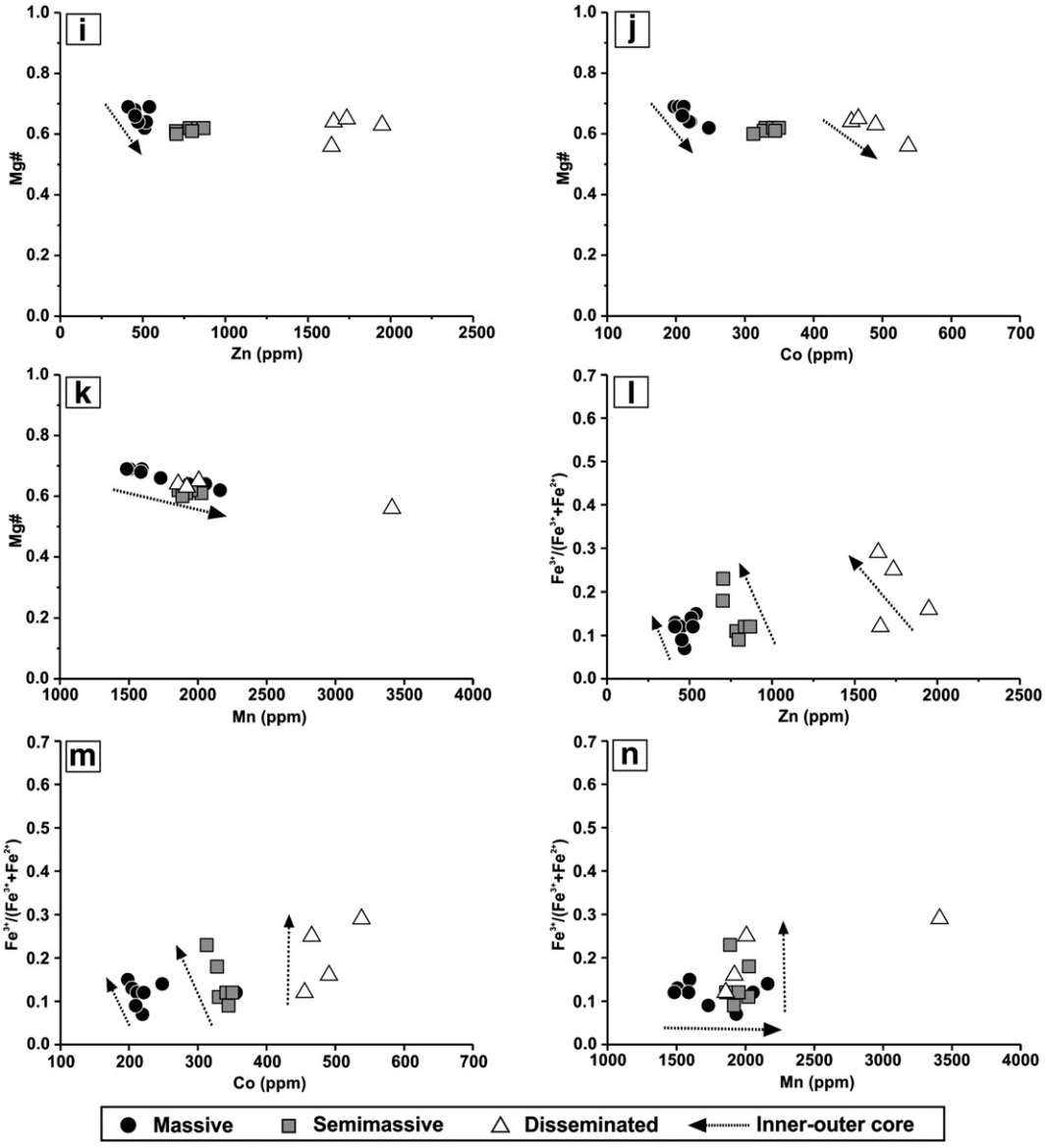

Fig. 8 (*continued*).

differences can be explained by the re-ordering of Fe^{2+} and Fe^{3+} in octahedral sites in the non-porous ferrian chromite rims, which limits the uptake of Ga^{3+}, Ni^{2+} and Sc^{3+} but allows the diffusion of Zn, Co (and Mn) toward the cores (Fig. 6). The Ti contents in cores of the zoned chromites of Yakovitsa are lower than those of the partly altered chromite, suggesting that in samples from small chromitite bodies (<20 cm thick) and with lower chromite/silicate ratios, Ti^{4+} also diffuses from core to rim (Fig. 6).

6. Conclusions

(1) Eclogite- to amphibolite-facies retrograde metamorphism has produced four microstructural types of chromite in the Rhodopean chromitites: (1) *porous chromite*, enriched in Cr and Fe^{2+} and depleted in Al, with chlorite filling the pores; (2) *partly altered chromite*, with primary cores surrounded by porous chromite; (3) *non-porous chromite*, enriched in Fe^{3+} (i.e. ferrian chromite) with polygonal mosaic microstructure, and (4) *zoned chromite*, with primary cores surrounded by non-porous chromite.

(2) High-Cr cores and porous rims surrounding them in partly altered chromites are enriched in Zn, Co and Mn (ZCM-anomaly) and depleted in Ga, Ni and Sc. This distribution of minor- and trace elements is the result of the exchange (i.e., diffusion) of minor- and trace elements between cores and their surrounding rims (with higher contents of Ga, Ti, Ni Mn, and Sc, but lower in V) concomitant with the crystallization of chlorite in the pores. We propose this ZCM-anomaly as a fingerprint of amphibolite-facies metamorphism.

(3) High-Al cores of partly altered chromites and their thin surrounding porous rims show identical trace-element patterns, which suggest a more limited reaction between these cores and infiltrating reducing fluids. Such a limited exchange of elements does not substantially modify the original composition in chromite cores.

(4) Small grains of high-Al porous chromite are significantly more enriched in Zn, Co and Mn (ZCM-anomaly) and depleted in Ga, Ni, Sc and V than rims on partly altered chromite. This suggests greater element mobility as a result of almost complete infiltration of altering fluids.

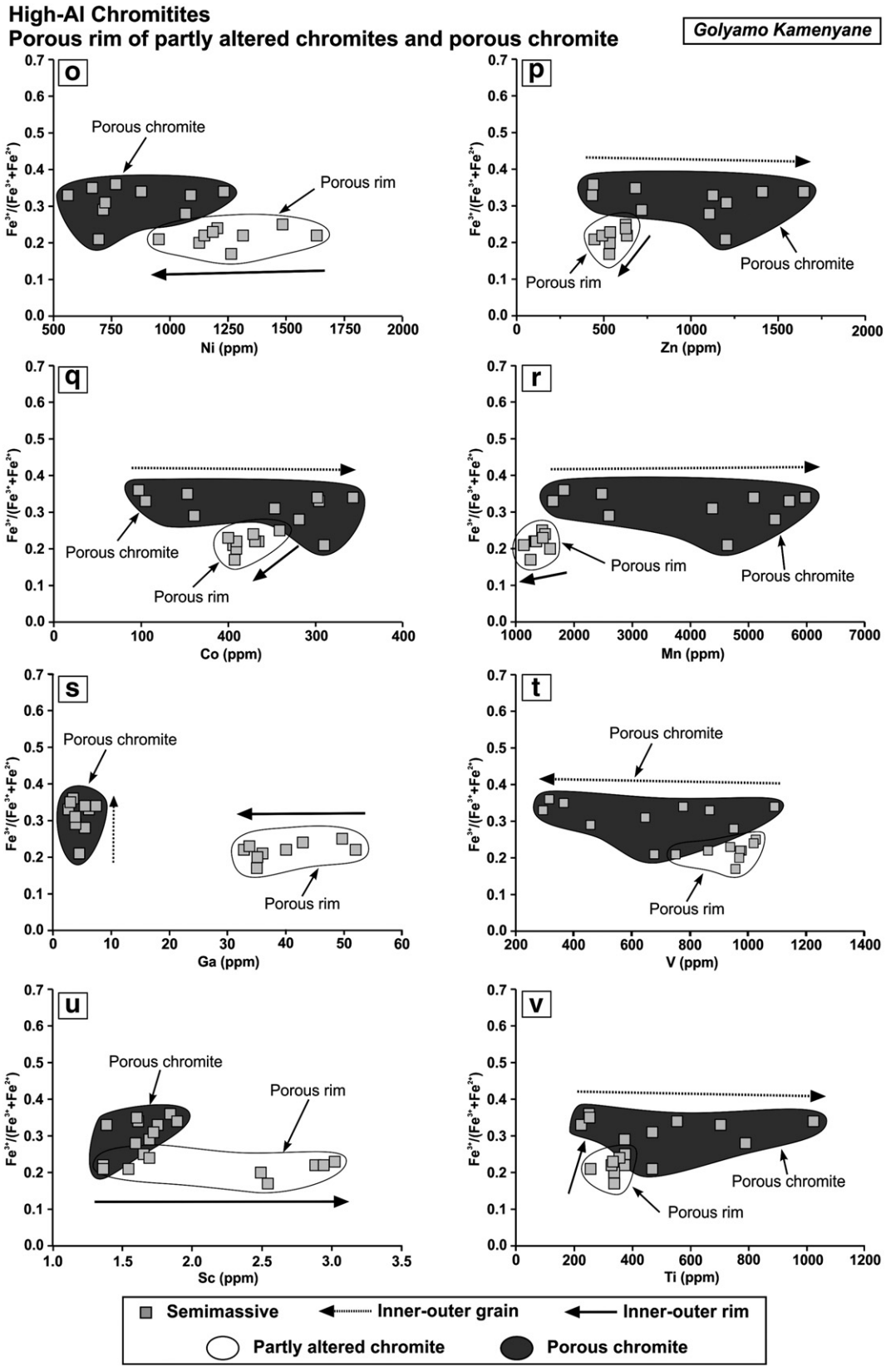

Fig. 8 (*continued*).

(5) Non-porous chromite grains and rims on cores of zoned chromite in high-Cr and high-Al chromitites exhibit similar patterns of minor- and trace elements, suggesting their equilibration with a common oxidizing fluid. This fluid, rich in the magnetite component, has obliterated the geochemical signatures of the pre-existing chromite regardless of its original composition.

(6) Within a single ultramafic massif, the cores of zoned chromite grains show a distinctive pattern (depleted in Ga, Ni and Sc but

enriched in Zn and Co, relative to non-porous rims) different from the cores of partly altered chromite grains. This reflects the interaction of chromite cores with rims formed by a distinct type of fluid (i.e. Fe^{2+}-rich in the porous chromite vs Fe^{3+}-rich in the non-porous chromite).

(7) This study reveals that the in-situ analysis of minor- and trace elements in chromite using LA-ICP-MS may help to recognize fingerprints of metamorphism. This is valuable information that may limit incorrect interpretations of the petrogenesis of the chromite host rocks. Additionally, the metamorphic fingerprints identified in this paper can be applied to the study of isolated chromite grains in serpentinites elsewhere. We expect that the disturbance of trace- and minor elements by metamorphism is much more effective in chromites from peridotites than in chromitites, as the former have lower chromite/silicate ratios that allow higher rates of reaction between infiltrating fluid and chromite. Very likely it would result in more complex patterns than those observed here. This suggestion can be the basis of future studies.

Supplementary data to this article can be found online at http://dx.doi.org/10.1016/j.chemgeo.2014.10.001.

Acknowledgments

This paper is a contribution to project CGL2010-15171 and F.P.I. grant BES-2011-045423 of the Spanish Ministry of Economy and Competitiveness. We would also like to thank Ibrahim Uysal and an anonymous reviewer for their comments that helped clarify the text of this manuscript. The analytical data were obtained using instrumentation funded by DEST Systemic Infrastructure Grants, ARC LIEF, NCRIS, industry partners and Macquarie University. This is a contribution 504 from the ARC Centre of Excellence for Core to Crust Fluid Systems (http://www.ccfs.mq.edu.au) and 958 in the GEMOC Key Centre (http://www.gemoc.mq.edu.au).

References

Abzalov, M.Z., 1998. Chrome–spinels in gabbro–wehrlite intrusions of the Pechenga area, Kola Peninsula, Russia: emphasis on alteration features. Lithos 43 (3), 109–134.

Ahmed, A.H., Arai, S., Abdel-Aziz, Y.M., Rahimi, A., 2005. Spinel composition as a petrogenetic indicator of the mantle section in the Neoproterozoic Bou Azzer ophiolite, Anti-Atlas, Morocco. Precambrian Res. 138 (3), 225–234.

Aldanmaz, E., 2012. Trace element geochemistry of primary mantle minerals in spinel-peridotites from polygenetic MOR–SSZ suites of SW Turkey: constraints from an LA-ICP-MS study and implications for mantle metasomatism. Geol. J. 47 (1), 59–76.

Allen, D.E., Seyfried Jr., W., 2003. Compositional controls on vent fluids from ultramafic-hosted hydrothermal systems at mid-ocean ridges: an experimental study at 400 °C, 500 bars. Geochim. Cosmochim. Acta 67 (8), 1531–1542.

Alt, J.C., Shanks, W.C., 1998. Sulfur in serpentinized oceanic peridotites: serpentinization processes and microbial sulfate reduction. J. Geophys. Res. Solid Earth 103 (B5), 9917–9929.

Alt, J.C., Shanks, W.C., Bach, W., Paulick, H., Garrido, C.J., Beaudoin, G., 2007. Hydrothermal alteration and microbial sulfate reduction in peridotite and gabbro exposed by detachment faulting at the Mid-Atlantic Ridge, 15°20′N (ODP Leg 209): a sulfur and oxygen isotope study. Geochem. Geophys. Geosyst. 8 (8), Q08002.

Arai, S., 1992. Chemistry of chromian spinel in volcanic rocks as a potential guide to magma chemistry. Mineral. Mag. 56 (383), 173–184.

Bach, W., Garrido, C.J., Paulick, H., Harvey, J., Rosner, M., 2004. Seawater-peridotite interactions: first insights from ODP Leg 209, MAR 15°N. Geochem. Geophys. Geosyst. 5 (9), Q09F26.

Bach, W., Paulick, H., Garrido, C.J., Ildefonse, B., Meurer, W.P., Humphris, S.E., 2006. Unraveling the sequence of serpentinization reactions: petrography, mineral chemistry, and petrophysics of serpentinites from MAR 15°N (ODP Leg 209, Site 1274). Geophys. Res. Lett. 33 (13), L13306.

Barnes, S.J., 2000. Chromite in komatiites, II. Modification during greenschist to mid-amphibolite facies metamorphism. J. Petrol. 41 (3), 387.

Barnes, S.J., Roeder, P.L., 2001. The range of spinel compositions in terrestrial mafic and ultramafic rocks. J. Petrol. 42 (12), 2279.

Bazylev, B.A., Zakariadze, G., Zhelyazkova-Panayotova, M., Kolcheva, K., Oberhaensli, R., Solov'eva, N., 1999. Petrology of ultramafic rocks from the ophiolite association in the crystalline basement of the Rhodope massif. Petroleum 7, 192–211.

Bliss, N., MacLean, W., 1975. The paragenesis of zoned chromite from central Manitoba. Geochim. Cosmochim. Acta 39 (6), 973–990.

Bonev, N., 2006. Cenozoic tectonic evolution of the Eastern Rhodope massif (Bulgaria): basement structure and kinematics of syn- to post-collisional extensional deformation. In: Dilek, Y., Paulides, S. (Eds.), Mediterranean Region and Asia. Geol. Soc. Am. Spec. Paper 49, pp. 211–235.

Bonev, N., Peychev, K., Nizamova, D., 2006. MOR- vs. SSZ-origin of metamafic rocks in the upper high-grade basement unit of the eastern Rhodope: geochemical diversity and tectonic significance. Proceedings of Annual Conference of the Bulgarian Geological Society, Geosciences 2006, pp. 181–184.

Burkhard, D.J.M., 1993. Accessory chromium spinels: their coexistence and alteration in serpentinites. Geochim. Cosmochim. Acta 57 (6), 1297–1306.

Candia, M., Gaspar, J., 1997. Chromian spinels in metamorphosed ultramafic rocks from Mangabal I and II complexes, Goiás, Brazil. Mineral. Petrol. 60 (1), 27–40.

Cassard, D., Nicolas, A., Rabinovitch, M., Moutte, J., Leblanc, M., Prinzhofer, A., 1981. Structural classification of chromite pods in southern New Caledonia. Econ. Geol. 76 (4), 805–831.

Daieva, L., Haydoutov, I., Pristavova, S., 2007. Geochemical correlation of metabasic rocks from Central and East Rhodopes, Bulgaria. Geochim. Mineral. Petrol. 45, 109–118.

Dare, S.A.S., Pearce, J.A., McDonald, I., Styles, M.T., 2009. Tectonic discrimination of peridotites using fO_2–Cr# and Ga–Ti–Fe^{III} systematics in chrome–spinel. Chem. Geol. 261 (3–4), 199–216.

Dick, H.J.B., Bullen, T., 1984. Chromian spinel as a petrogenetic indicator in abyssal and alpine-type peridotites and spatially associated lavas. Contrib. Mineral. Petrol. 86 (1), 54–76.

Droop, G., 1987. A general equation for estimating Fe_3 concentrations in ferromagnesian silicates and oxides from microprobe analyses, using stoichiometric criteria. Mineral. Mag. 51 (361), 431–435.

Evans, B.W., Frost, B.R., 1975. Chrome–spinel in progressive metamorphism—a preliminary analysis. Geochim. Cosmochim. Acta 39 (6–7), 959–972.

Frost, B.R., 1991. Stability of oxide minerals in metamorphic rocks. In: Lindsley, H.R. (Ed.), Oxide Minerals: Petrologic and Magmatic Significance. Mineral. Soc. Am. Rev. Mineral 25, pp. 469–487.

Gao, S., Liu, X., Yuan, H., Hattendorf, B., Günther, D., Chen, L., Hu, S., 2002. Determination of forty two major and trace elements in USGS and NIST SRM glasses by laser ablation-inductively coupled plasma-mass spectrometry. Geostand. Newslett. 26 (2), 181–196.

Georgiev, V., 2006. Tertiary domes and depressions in the Rhodope massif. Proceedings of Annual Conference of the Bulgarian Geological Society, Geosciences 2006, pp. 106–109.

Gervilla, F., Padrón-Navarta, J., Kerestedjian, T., Sergeeva, I., González-Jiménez, J., Fanlo, I., 2012. Formation of ferrian chromite in podiform chromitites from the Golyamo Kamenyane serpentinite, Eastern Rhodopes, SE Bulgaria: a two-stage process. Contrib. Mineral. Petrol. 164, 1–15.

González Jiménez, J.M., Kerestedjian, T., Proenza Fernández, J.A., Gervilla Linares, F., 2009. Metamorphism on chromite ores from the Dobromirtsi ultramafic massif, Rhodope Mountains (SE Bulgaria). Geol. Acta 7 (4), 413–429.

González-Jiménez, J.M., Augé, T., Gervilla, F., Bailly, L., Proenza, J.A., Griffin, W.L., 2011. Mineralogy and geochemistry of platinum-rich chromitites from the mantle–crust transition zone at Ouen Islad, New Caledonia Ophiolite. Can. Mineral. 49 (6), 1549–1569.

González-Jiménez, J.M., Locmelis, M., Belousova, E., Griffin, W.L., Gervilla, F., Kerestedjian, T.N., Pearson, N.J., Sergeeva, I., 2013. Genesis and tectonic implications of podiform chromitites in the metamorphosed Ultramafic Massif of Dobromirtsi (Bulgaria). Gondwana Res. http://dx.doi.org/10.1016/j.gr.2013.09.020.

González-Jiménez, J.M., Griffin, W.L., Gervilla, F., Proenza, J.A., O'Reilly, S.Y., Pearson, N.J., 2014. Chromitites in ophiolites: how, where, when, why? Part II. The crystallization of chromitites. Lithos 189, 140–158.

Grieco, G., Merlini, A., 2012. Chromite alteration processes within Vourinos ophiolite. Int. J. Earth Sci. 101 (6), 1523–1533.

Griffin, W., O'Reilly, S.Y., Afonso, J.C., Begg, G., 2009. The composition and evolution of lithospheric mantle: a re-evaluation and its tectonic implications. J. Petrol. 50 (7), 1185–1204.

Haydoutov, I., Kolcheva, K., Daieva, L., Savov, I., 2001. Island-arc origin of the neoproterozoic variegated formations from the east Rhodopes (Avren synform and Bela Reka antiform), Bulgaria. EUROPROBE Meeting, METU, Ankara, Abs. 1, pp. 31–32.

Haydoutov, I., Kolcheva, K., Daieva, L., Savov, I., Carrigan, C., 2004. Island arc origin of the variegated formations from the east Rhodope, Bulgaria-implications for the evolution of the Rhodope massif. Ofioliti 29 (2), 145–157.

Irvine, T., 1967. Chromian spinel as a petrogenetic indicator: part 2. Petrologic applications. Can. J. Earth Sci. 4 (1), 71–103.

Jan, M.Q., Windley, B.F., 1990. Chromian spinel-silicate chemistry in ultramafic rocks of the Jijal complex, Northwest Pakistan. J. Petrol. 31 (3), 667–715.

Janák, M., Froitzheim, N., Georgiev, N., Nagel, T., Sarov, S., 2011. P–T evolution of kyanite eclogite from the Pirin Mountains (SW Bulgaria): implications for the Rhodope UHP Metamorphic Complex. J. Metamorph. Geol. 29 (3), 317–332.

Kamenetsky, V.S., Crawford, A.J., Meffre, S., 2001. Factors controlling chemistry of magmatic spinel: an empirical study of associated olivine, Cr-spinel and melt inclusions from primitive rocks. J. Petrol. 42 (4), 655–671.

Kimball, K.L., 1990. Effects of hydrothermal alteration on the composition of chromian spinels. Contrib. Mineral. Petrol. 105, 337–346.

Kolcheva, K., Eskenazy, G., 1988. Geochemistry of metaeclogites from the central and eastern Rhodope Mts (Bulgaria). Geol. Balc. 18 (5), 61–78.

Kolcheva, K., Haydoutov, I., Daieva, L., 2000. Dismembered ultramafic ophiolites from the Avren synform, Eastern Rhodopes. Geochem. Mineral. Petrol. 37, 25–38.

Kolkovski, B., Petrov, P., Dobrev, S., 2003. Hydrothermal ore-bearing features of igneous intrusive complexes. Geol. Geophys. 46 (1), 65–76.

Kozhoukharov, D., Kozhoukharova, E., Papanikolaou, D., 1988. Precambrian in the Rhodope massif. In: Zoubek, V. (Ed.), Precambrian in Younger Fold Belts: European Variscides, the Carpathians, and Balkans. International Geological Correlation Programme, Project 22. Wiley, Chichester, pp. 773–778.
Leblanc, M., Nicolas, A., 1992. Ophiolitic chromitites. Int. Geol. Rev. 34 (7), 653–686.
Leblanc, M., Dupuy, C., Cassard, D., Moutte, J., Nicolas, A., Prinzhoffer, A., Rabinovitch, M., Routhier, P., 1980. Essai sur la genèse des corps podiformes de chromitite dans les péridotites ophiolitiques de Nouvelle-Calédonie et de Méditerranée orientale. In: Panayiotou, A. (Ed.), Ophiolites: Proceedings of the International Ophiolite Symposium, Nicosia, Cyprus, 1979. Geol. Seurv. Dep. Nicossia, Cyprus, pp. 692–701.
Locmelis, M., Pearson, N.J., Barnes, S.J., Fiorentini, M.L., 2011. Ruthenium in komatiitic chromite. Geochim. Cosmochim. Acta 75, 3645–3661.
Loferski, J.P., 1986. Petrology of metamorphosed chromite-bearing ultramafic rocks from the Red Lodge District. USGS Bull., Professional Paper 44.
Mellini, M., Rumori, C., Viti, C., 2005. Hydrothermally reset magmatic spinels in retrograde serpentinites: formation of "ferritchromit" rims and chlorite aureoles. Contrib. Mineral. Petrol. 149 (3), 266–275.
Merlini, A., Grieco, G., Diella, V., 2009. Ferritchromite and chromian-chlorite formation in mélange-hosted Kalkan chromitite (Southern Urals, Russia). Am. Mineral. 94 (10), 1459–1467.
Mposkos, E., 2002. Petrology of the ultra-high pressure metamorphic Kimi complex in Rhodope (NE Greece): a new insight into the Alpine geodynamic evolution of the Rhodope. Bull. Geol. Soc. Greece 34, 2169–2188.
Mposkos, E., Krohe, A., 2000. Petrological and structural evolution of continental high pressure (HP) metamorphic rocks in the Alpine Rhodope Domain (N. Greece). In: Panaydes, I., Xenopontos, C., Malpas, J. (Eds.), Proceedings of the 3rd International Conference on the Geology of the Eastern Mediterranean (Nicosia, Cyprus). Geol. Surv. Cyprus, pp. 221–232.
Mposkos, E., Krohe, A., 2006. Pressure–temperature–deformation paths of closely associated ultra-high-pressure (diamond-bearing) crustal and mantle rocks of the Kimi complex: implications for the tectonic history of the Rhodope Mountains, northern Greece. Can. J. Earth Sci. 43 (12), 1755–1776.
Mposkos, E., Baziotis, I., Proyer, A., 2012. Pressure–temperature evolution of eclogites from the Kechros complex in the Eastern Rhodope (NE Greece). Int. J. Earth Sci. 101 (4), 973–996.
Mukherjee, R., Mondal, S.K., Rosing, M.T., Frei, R., 2010. Compositional variations in the Mesoarchean chromites of the Nuggihalli schist belt, Western Dharwar Craton (India): potential parental melts and implications for tectonic setting. Contrib. Mineral. Petrol. 160 (6), 865–885.
Norman, M., Pearson, N., Sharma, A., Griffin, W., 1996. Quantitative analysis of trace elements in geological materials by laser ablation ICPMS: instrumental operating conditions and calibration values of NIST glasses. Geostand. Newslett. 20 (2), 247–261.
Olobaniyi, S.B., Mücke, A., 2011. Chemical composition of chromite and intergrown chlorite in metamorphosed ultramafic rocks (serpentinite and talc schist) of the Egbe-Isanlu schist belt, southwest Nigeria: genetic implications. J. Min. Geol. 47 (2), 115–134.
Pagé, P., Barnes, S.J., 2009. Using trace elements in chromites to constrain the origin of podiform chromitites in the Thetford Mines ophiolite, Québec, Canada. Econ. Geol. 104 (7), 997–1018.
Proenza, J., Ortega-Gutiérrez, F., Camprubí, A., Tritlla, J., Elías-Herrera, M., Reyes-Salas, M., 2004. Paleozoic serpentinite-enclosed chromitites from Tehuitzingo (Acatlán Complex, southern Mexico): a petrological and mineralogical study. J. S. Am. Earth Sci. 16 (8), 649–666.
Proenza, J., Zaccarini, F., Escayola, M., Cábana, C., Schalamuk, A., Garuti, G., 2008. Composition and textures of chromite and platinum-group minerals in chromitites of the western ophiolitic belt from Pampean Ranges of Córdoba, Argentina. Ore Geol. Rev. 33 (1), 32–48.
Rollinson, H., 2008. The geochemistry of mantle chromitites from the northern part of the Oman ophiolite: inferred parental melt compositions. Contrib. Mineral. Petrol. 156 (3), 273–288.
Rollinson, H., Appel, P.W.U., Frei, R., 2002. A metamorphosed, early Archaean chromitite from west Greenland: implications for the genesis of Archaean anorthositic chromitites. J. Petrol. 43 (11), 2143–2170.
Sack, R.O., Ghiorso, M.S., 1991. Chromian spinels as petrogenetic indicators — thermodynamics and petrological applications. Am. Mineral. 76 (5–6), 827–847.
Satsukawa, T., González-Jiménez, J.M., Colás, V., Griffin, W.L., Piazolo, S., O'Reilly, S.Y., Gervilla, F., Fanlo, I., 2014. Fluid-induced deformation in chromite during metamorphism. Proceedings of 6th Orogenic Lherzolite Conference, Marrakech 2014.
Singh, A.K., Singh, R.B., 2013. Genetic implications of Zn- and Mn-rich Cr-spinels in serpentinites of the Tidding Suture Zone, eastern Himalaya, NE India. Geol. J. 48 (1), 22–38.
Stowe, C.W., 1994. Compositions and tectonic settings of chromite deposits through time. Econ. Geol. 89 (3), 528–546.
Wylie, A.G., Candela, P.A., Burke, T.M., 1987. Compositional zoning in unusual Zn-rich chromite from the Sykesville district of Maryland and its bearing on the origin of "ferritchromit". Am. Mineral. 72 (3–4), 413–422.
Zhou, M., Robinson, P.T., 1994. High-Cr and high-Al podiform chromitites, Western China: relationship to partial melting and melt/rock reaction in the upper mantle. Int. Geol. Rev. 36 (7), 678–686.